AD_____

AD-A210 384

SPATIAL RELATIONSHIPS BETWEEN DRUG BINDING SITES ON THE SURFACE OF THE ACETYLCHOLINE RECEPTOR

Annual Report

David A. Johnson, Ph.D.

October 15, 1987

Supported by

U.S. ARMY MEDICAL RESEARCH AND DEVELOPMENT COMMAND
Fort Detrick, Frederick, Maryland 21701-5012

Contract No. DAMD17-84-C-4187

University of California-Riverside
Riverside, California 92521-0121

DOD DISTRIBUTION STATEMENT

Approved for public release; distribution unlimited

SECURITY CLASSIFICATION OF THIS PAGE

REPORT DOCUMENTATION PAGE

Form Approved
OMB No. 0704-0188

1a. REPORT SECURITY CLASSIFICATION: Unclassified	1b. RESTRICTIVE MARKINGS
2a. SECURITY CLASSIFICATION AUTHORITY	3. DISTRIBUTION/AVAILABILITY OF REPORT: Approved for public release; distribution unlimited
2b. DECLASSIFICATION/DOWNGRADING SCHEDULE	
4. PERFORMING ORGANIZATION REPORT NUMBER(S)	5. MONITORING ORGANIZATION REPORT NUMBER(S)
6a. NAME OF PERFORMING ORGANIZATION: University of California-Riverside; 6b. OFFICE SYMBOL (If applicable)	7a. NAME OF MONITORING ORGANIZATION
6c. ADDRESS (City, State, and ZIP Code): Riverside, California 92521-0121	7b. ADDRESS (City, State, and ZIP Code)
8a. NAME OF FUNDING/SPONSORING ORGANIZATION: U.S. Army Medical Research & Development Command; 8b. OFFICE SYMBOL (If applicable)	9. PROCUREMENT INSTRUMENT IDENTIFICATION NUMBER: Contract No. DAMD17-84-C-4187
8c. ADDRESS (City, State, and ZIP Code): Fort Detrick, Frederick, Maryland 21701-5012	10. SOURCE OF FUNDING NUMBERS

PROGRAM ELEMENT NO.	PROJECT NO.	TASK NO.	WORK UNIT ACCESSION NO.
62734A	3M1-62734A875	AI	457

11. TITLE (Include Security Classification)

Spatial Relationships Between Drug Binding Sites on the Surface of the Acetylcholine Receptor

12. PERSONAL AUTHOR(S)

David A. Johnson, Ph.D.

13a. TYPE OF REPORT	13b. TIME COVERED	14. DATE OF REPORT (Year, Month, Day)	15. PAGE COUNT
Annual Report	FROM 9/15/86 TO 9/14/87	1987 October 15	109

16. SUPPLEMENTARY NOTATION

17. COSATI CODES			18. SUBJECT TERMS (Continue on reverse if necessary and identify by block number)
FIELD	GROUP	SUB-GROUP	Acetylcholine receptor, cobra a-toxin, fluorescein isothiocyanate, ethidium, anesthetics, fluorescence, RA V

19. ABSTRACT (Continue on reverse if necessary and identify by block number)

This report is divided into three sections dealing with the development and use of fluorescent probes of the nicotinic acetylcholine receptor (AcChR). Section I summarized the purification and characterization of four mono-fluorescein cobra a-toxin derivatives. Section II deals with the use of the about derivatives to define the approximate orientation of cobra a-toxin on the acetylcholine receptor. Section III summarizes our measurements of the intersite distances between the binding sites for acetylcholine and phencyclidine on the nicotinic acetylcholine receptor.

20. DISTRIBUTION/AVAILABILITY OF ABSTRACT	21. ABSTRACT SECURITY CLASSIFICATION
☐ UNCLASSIFIED/UNLIMITED ☒ SAME AS RPT. ☐ DTIC USERS	Unclassified

22a. NAME OF RESPONSIBLE INDIVIDUAL	22b TELEPHONE (Include Area Code)	22c. OFFICE SYMBOL
Mrs. Virginia M. Miller	301/663-7325	SGRD-RMI-S

SUMMARY

This report is divided into three sections dealing with the development and use of fluorescent probes of the nicotinic acetylcholine receptor (AcChR). Section I summarized the purification and characterization of four mono-fluorescein cobra α-toxin derivatives. Section II deals with the use of the about derivatives to define the approximate orientation of cobra α-toxin on the acetylcholine receptor. Section III summarizes our measurements of the intersite distances between the binding sites for acetylcholine and phencyclidine on the nicotinic acetylcholine receptor.

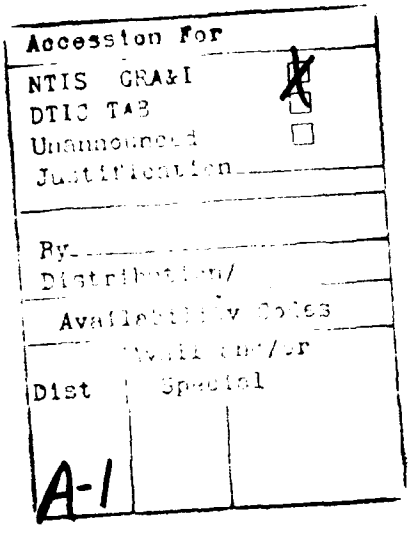

FOREWORD

In conducting research using animals, the investigator(s) adhered to the "Guide for the Care and Use of Laboratory Animals," prepared by the Committee on Care and Use of Laboratory Animals of the Institute of Laboratory Animal Resources, National Research Council (NIH Publication No. 86-23, Revised 1985).

Citations of commercial organizations and trade names in this report do not constitute an official Department of the Army endorsement or approval of the products or services of these organizations.

TABLE OF CONTENTS

List of Figures

List of Tables

Section I

PURIFICATION AND CHARACTERIZATION OF FOUR MONO-FLUORESCEIN COBRA α-TOXIN DERIVATIVES

INTRODUCTION

Radionuclide and fluorescent labeled snake α-toxins have played an important role in the identification and characterization of nicotinic acetylcholine receptors. Much information has been obtained without a knowledge of the site(s) of labelling. However, additional insights, particularly with fluorescent labeled α-toxins, concerning the structure and dynamics of the nicotinic acetylcholine receptor (AcChR) and the nature of the interaction of the α-toxin with the receptor, can be achieved with characterized mono-fluorescent labeled derivatives. We have previously reported the isolation and characterization of Nεfluorescein lysine 23 α-toxin (FITC-lys-23-toxin). With this derivative we evaluated the solute accessibility to the region about lys 23 with the α-toxin free in solution and bound to the receptor (Cheung, et al., 1984). With FITC-lys-23-toxin, we also estimated the distance between the two α-toxin binding sites on the surface of the AcChR (Johnson et al., 1984). The information provided by the solute accessibility studies was necessarily limited to the region about lys 23, and the interpretation of the data from the inter-α-toxin site distance measurements was limited by the uncertainty in location of the fluorophore relative to the orientation of the bound α-toxin

molecule. Clearly, greater information on solute accessibility to other regions of the α-toxin and on the orientation of α-toxin molecules relative to each other on the surface of the AcChR could be gained if other mono-fluorescent α-toxin derivatives were available. To obtain additional mono-fluorescein α-toxin derivatives, we purified four of the six possible mono-fluorescein α-toxin derivatives by isoelectric focusing in immobilized pH gradients (IPG) and characterized these derivatives, biochemically and spectroscopically.

EXPERIMENTAL PROCEDURES

Materials. Cobra α-toxin (siamensis 3) was isolated following the method of Karlsson et al., (1971) from Naja naja siamensis venom (Miami Serpentarium Salt Lake City, UT). [^{125}I]iodo-α-bungarotoxin was purchased from New England Nuclear (Boston, MA). Fluorescein-5-isothiocyanate (FITC) was purchased from Molecular Probes, Inc. (Eugene, OR). All other reagents were at least reagent grade. Except where noted, all binding and spectroscopic analyses were performed with samples suspended in 100mM NaCl, 10mM sodium phosphate buffer at pH 7.4.

Receptor Isolation. Receptor-enriched membrane fragments were isolated from Torpedo californica electric organ following published procedures (Johnson and Yguerabide, 1985; Reed et al., 1973). The specific binding activities of the receptor preparations were measured by adsorption of [125I]iodo-α-bungarotoxin receptor complexes onto DEAE-cellulose filters (Schmidt and Raftery, 1975) and ranged between 2 and 3.0 nmol of α-toxin binding sites/mg protein.

FITC Labelling of α-Toxin. Unless stated otherwise, 3.8 μmol citraconic anhydride in 10 μl methanol was incubated with 0.26 μmol α-toxin in 600 μl of sodium phosphate (220 mM)/ EDTA (0.175 mM) buffer at pH 10.5 for 2 h at room temperature (Lobel et al., 1985). The reaction was continued for an additional 30 min after the addition of 0.386 μmol FITC in 12 μl dimethylformamide. The

reaction mixture was dialyzed overnight (Mr 3500 cut-off tubing) at room temperature against 1 M acetic acid (1 L) and rotary evaporated to ~200ul.

Preparative Isoelectric Focusing in Immobilized pH Gradients. Preparative isoelectric focusing in IPG was performed using the LKB Immobiline system (LKB Application Notes No. 323 and 324). The following modifications were made: The recommended concentrations of the Immobilines were doubled. One pH unit gradients were formed by adjusting at room temperature the pH of the acidic, dense and basic, light solutions with the pK 9.3 Immobiline (0.0-1.4 ml). Batch variability of the Immobiline dictated adjusting the one unit pH gradients anywhere from 9.0-10.0 to 9.3-10.3 to obtain consistent migration patterns. Polymerized gels (11 x 11 x 0.5 cm) were immersed in 20% glycerol (w/v) for 14 to 16 h and dried to within one to two grams of the preglycerol treated weight with a hot air gun. The gels were focused using the LKB Ultrophor Electrofocusing Unit, with the electrodes placed directly on the gel. To prevent the electrodes from slicing the gel, rubber spacers were placed between the electrode holder and the cooling plate. After the gels were prefocused at 4°C for one hour with the LKB Macrodrive 5 power supply set at 20 watts, the FITC-toxin reaction mixture (2.5 μmol) was placed in a preformed well in the gel (68x7x2.5mm) and focused for six hours at a constant power of 10 watts (5000 V limiting). Focusing was continued for an additional 12 to 14 h at 5 watts (3500V limiting).

Protein Recovery from the IPG matrix. The focused fluorescent bands were visualized with a mineral lamp and excised with a razor blade. Each excised segment of gel was chopped into approximately 2 mm cubes and incubated with 25mls of cation exchange resin (Whatman carboxymethylcelluluse CM-52) for 2 to 3 days at 4°C. The resin was prepared as described elsewhere (Karlsson et al.,1972) and

equilibrated with ammonium acetate buffer (0.03 M at pH 4.8). The fluorescent proteins were eluted from the resin with 0.3 M ammonium acetate and the eluant rotary evaporated to 2-3 ml. Removal of gel contaminants and further purification of the mono-FITC-toxin derivatives was achieved by high pressure liquid chromatography (HPLC). HPLC gradients were formed by mixing 0.1% (w/v) trifluoroacetic acid (TFA) in H_2O and acetonitrile. With the exception of Band 5 satisfactory purifications were achieved by eluting the samples through Vydac C_{18} column (0.46x25 cm), equilibrated with a primary solvent system of 20% acetonitrile and running a linear 80-min gradient between this primary solvent and a secondary solvent of 40% acetonitrile at a flow rate of 1 ml/min. In addition to the above HPLC purification step, Band 5 was eluted through a Vydac diphenyl column (0.46 x 25 cm) equilibrated with a primary solvent of 0 % acetonitrile and eluted with two linear gradients. The first gradient started from this primary solvent to a secondary solvent of 15% acetonitrile over 15 min. The second gradient started where the first gradient ended and ran to 40% acetonitrile over 65 min at a flow rate of 0.75 ml/min. All HPLC separations were carried out at room temperature with a Beckman model 334 HPLC system.

Thermolysin Digestion and Peptide Mapping. Reduced and S-carboxymethylated FITC-toxin (1-2 nmol) was dissolved in 25 μl of 0.1 M NH_4HCO_3, 5 mM $CaCl_2$, pH 8.1. Thermolysin (1.6-3.2 μg) was added, incubated overnight at 37°C, and the sample evaporated to dryness with a Savant vacuum centrifuge. The fluorescent products of the digest were resolved with one, and sometimes two HPLC columns. Initially the digests were chromatographed on a Vydac C_{18} equilibrated with 0.1% (w/v) TFA and eluted with a gradient of 0 to 40% acetonitrile. When nonfluorescent peptides coeluted with fluorescent peptides, the nonfluorescent peptides were separated from the fluorescent peptides using a Vydac C_4 column

(0.46 x 25 cm) column eluted with a 20 to 40 % acetonitrile gradient.

Microsequence Analysis. Microsequence analysis of the fluorescent peptides (30-60 pmol) was performed on a Applied Biosystems Model 470-A gas-phase microsequencer. Phenthiohydantoin derivatives were analyzed on-line by reverse-phase, microbore HPLC. Repetitive yields of 69-75% were obtained.

Steady State Spectroscopy. Steady-state fluorescence and UV/visible spectral measurements were made with a Perkin-Elmer MPF-66 Spectrofluorometer and a Perkin-Elmer Lambda 3B Spectrophotometer, respectively. The quantum yields of the FITC-toxins were determined by the ratio method of Chen (1965). Since FITC contributes 0.05 to the extinction of native α-toxin in the Lowry protein assay (Lowry et al., 1951), the concentration of solutions of FITC-toxin for the determination of the molar extinction coefficients, ϵ, were measured by the Lowry method with native α-toxin as a standard.

Binding Kinetics. The binding kinetics of FITC-toxins were studied by monitoring the changes in fluorescence associated with binding of the toxins to the receptor. A detailed description of the procedures is presented elsewhere (Cheung et al., 1984). Briefly, using a Perkin-Elmer MPF-66 spectrofluorometer the time-dependent changes in fluorescence associated with the FITC-toxin-receptor binding were fitted to appropriate integrated rate expressions. Association kinetic data, generated by monitoring FITC fluorescence after mixing of FITC-toxin with AcChR, were fit to the following integrated rate expressions for a reversible bimolecular mechanism:

$$\left[\frac{[L]_o[R]_o}{[LR]_e} - [LR]_e\right]^{-1} \ln\left[\frac{[LR]_e\,[L]_o - \frac{[LR][LR]_e}{[R]_o}}{[L]_o([LR]_e - [LR])}\right] = k^1 t. \qquad (1)$$

where $[L]_o$ and $[R]_o$ are the initial concentrations of α-toxin and receptor (in α-toxin sites), [LR] and $[LR]_e$ are the concentrations of the toxin-receptor-complexes at time t and at equilibrium, respectively. k_1 is the bimolecular association rate constant. The dissociation data, generated by monitoring FITC-toxin fluorescence after the addition of excess native α-toxin to samples of FITC-toxin-AcChR complexes, were fit to the following integrated rate expression for a simple unimolecular dissociation mechanism:

$$\ln[LR] = -k_{-1}t + \ln[LR]_o \qquad (2)$$

where k_{-1} is the unimolecular dissociation rate constant and $[LR]_o$ is the initial concentration of receptor-toxin complex. The time-dependent changes in fluorescence (I) upon binding were fit to the above integrated rate expressions by substituting in the initial concentrations of reactants and the following expressions:

$$[L]_o = I_o \qquad (3)$$

$$[LR] = (I_f - I)/(I_f - I_b))[L]_o \qquad (4)$$

$$[LR]_e = ((I_f - I_e)/(I_f - I_b))[L]_o \qquad (5)$$

where the subscripts f, b, e, o represent respectively the free, bound, equilibrium, and initial values of the parameters. When this plot is linear, the rate constant is given by the slope. The ratio I_b/I_f was measured by monitoring the change in fluorescence associated with incremental amounts of AcChR-toxin sites, plotting the ratio I_e/I_o versus 1/[AcChR toxin sites] and interpolating I_b/I_f to infinite AcChR-toxin sites.

RESULTS

Preparation of FITC-labeled α-Toxins. To redirect the FITC labelling away from the hyperreactive α-toxin lys 23, we reversibly modified α-toxin with citraconic anhydride. The modified α-toxin was then labeled with near-stoichiometric quantities of FITC, treated with acid to remove the citraconic anhydride, dialyzed, concentrated, and focused in one pH unit (9.0-10.0 to 9.3-10.3) IPG gels. The left panel of Fig. 1 shows a fluorescence photograph of one of these gels and a density scan of the photograph negative. Five, and sometimes six consistently spaced fluorescent bands focused between the cathode and anode and are referred to as Bands 1 to 6, respectively. Poly-FITC-conjugated α-toxins and monoconjugated FITC focused at the anode, while native α-toxin focused at the cathode (data not shown). Some tailing appeared from Band 6 into adjacent Bands 4 and 5. We could not determine the pH gradient of the gels, because the pH gradient is maintained by a modification of the poly acrylamide gel. Consequently, efforts to measure the pH of homogenized serial sections of the gel or to utilize a surface pH electrode were unsuccessful. We estimated the pIs of Band 1 and 6 to be ~9.3 and ~9.6, respectively, because we previously observed (Johnson and Taylor, 1983) that on an isoelectrofocusing column mono-FITC-toxin derivatives focus between pH 9.3 and 9.6.

Sufficient material was associated with the FITC-toxin monoconjugate Bands 1, 2, 3, 5, and 6 to attempt isolation and sequencing. These bands were extricated from the gel by adsorption onto cation exchange resin. The monoconjugates were eluted from the resin with a high ionic strength buffer. Significant amounts of glycerol and other gel contaminants from the IPG gel eluted with the mono-FITC derivatives, even when the gel-resin mixture was placed in a column and eluted with shallow salt gradient (data not shown). Consequently, the mono-FITC

derivatives were purified further by reverse phase HPLC. Elution profiles of fluorescence of Bands 1, 2, 3, and 6 and the elution profile of 280 nm extinction of native α-toxin are shown in Fig. 2. While our HPLC protocol did not resolve all the mono-FITC derivatives, native α-toxin eluted before the FITC-toxins and band 6 eluted before Bands 2, 3, and 5. (Band 5 profile not shown). Consequently, trace native α-toxin and Band 6 contaminates were removed from Band 2, 3, and 5 samples. To estimate final purity, the HPLC-purified Bands 1, 2, 3, and 6 were focused on an IPG. Based on fluorescence, Bands 1, 2, 3, and 6 were greater than 95% pure (Right Panel, Fig. 1). Band 5, though chromatographically homogeneous on IPG and reverse phase HPLC systems described above, is not shown because microsequencing indicated that Band 5 contained more than one mono-FITC derivative.

Protein Recovery. In separate experiments the recoveries of known amounts of FITC-toxin from the IPG gel and the HPLC column were determined to be 71 and 73%, respectively (data not shown). Also, by separation of FITC-labeled from unlabeled α-toxin with HPLC, we determined that 35% of the α-toxin was labeled after the citraconic anhydride treatment and 68% without citraconic anhydride treatment (data not shown).

The effect of citraconic anhydride modification on the pattern of FITC monolabeling was estimated from density scans of photograph negatives of the IPG and corrected for quantum yield and extinction of the Bands. These results are summarized in Table I. Citraconic anhydride modification reduced the labelling of Band 6 (from 85 to 68%) and increased the labelling of Bands 1 to 5. The labelling of Band 1 showed the greatest percent increase (from 7 to 20%).

Identification of Sites of Labelling. Bands 1, 2, 3, and 5 were reduced, S-carboxymethlyated, digested with thermolysin, and resolved on a C_{18} reverse

phase HPLC. Elution profiles of digests of Bands 1, 2, and 3 on a C_{18} reverse phase column showed only one major fluorescent peak (Figs. 3-5). Sequencing of the fractions associated with the major fluorescent peptide of Band 2 yielded an unambiguous sequence with a linear log recovery versus cycle number plot to be arg-"blank"-arg-pro. A "blank" represented a cycle with no detectable amino acid and suggested the presence of Nε-FITC-lys, since Nε-FITC-lys did not elute from the sequencing column with the solvent gradients used. (This was further supported by the sequencing of FITC-conjugated polylysine. Only lys was detected off of the column, data not shown). The uniqueness of the arg-"blank"-arg-pro sequence to the region about lys 69 suggests the site of labelling of Band 2 to be lys 69. The peak fluorescent fractions of digests of Bands 1 and 3 were rechromatographed on a C_4 reverse phase column to remove nonfluorescent peptides, that made sequencing equivocal. The rechromatographed fluorescent peaks also displayed single major peaks of fluorescence suggesting homogeneity of the fluorescent peptides associated with the digests of Bands 1 and 3. Sequencing of the fluorescent fractions associated with the rechromatographed major fluorescent peaks from the digestion of Bands 1 and 3 yielded unambiguous sequences with linear log recovery versus cycle number plots of ile-arg-gly-"blank"-arg and val-"blank"-gly, respectively (Top Panel, Figs. 3 and 5). The uniqueness of these sequences in the α-toxin sequence (Fig. 6) suggests that Band 1 was labeled at lys 35 and Band 3 at lys 49. Elution pro files of digests of Band 5 showed at least two major fluorescent peaks eluted from a C_{18} column based on seven determinations. The sequence of one of the fluorescent peptides of Band 5 suggested labelling at lys 12. The other major peak of fluorescence could not be sequenced and suggested that the N-terminus was blocked. These results indicated that Band 5 was a mixture of α-toxin labeled at

lysine 12 and at the N-terminus (ile 1). Because we were unable to resolve these derivatives, we focused our attention on characterizing only the isolated mono-FITC derivatives (Bands 1, 2, 3, and 6).

The site of labelling of Band 6 was determined to be lys 23 because Band 6 displayed essentially identical chromatographic, spectroscopic, and binding kinetic properties as our previously identified FITC-lys-23-toxin (Johnson and Taylor, 1983). Band 6 and FITC-lys-23-toxin focused at the same pI on a 9.0-10.0 IPG gel and displayed the same retention time on reverse phase HPLC (data not shown). The absorbance and emission maxima in NaCl-phosphate buffer (pH 7.4) were identical, 494 and 519, respectively. Both Band 6 and FITC- lys-23-toxin showed the same magnitude of fluorescence enhancement upon binding to the AcChR, 95 and 96%, respectively (Table II; Johnson and Taylor, 1982). The quantum yields and molar extinction coefficients of Band 6 and FITC- lys-23-toxin also were essentially identical, .18 versus .16 and 62,000 versus 55,000 $M^{-1}s^{-1}$, respectively (Table II and Johnson and Taylor, 1983). Finally, the association rate constants of Band 6 ($15 \times 10^3 M^{-1}s^{-1}$) and FITC-lys-23-toxin (6.7×10^3 $M^{-1}s^{-1}$) were within a factor of two of one another, and the dissociation rate constants differed by less than 6% (3.5×10^{-5} versus 3.3×10^{-5} s^{-1}, respectively) (Table III and Cheung et al., 1984).

Spectral Characterization. The absorption spectra and fluorescence emission spectra of the four isolated mono-FITC derivatives free in solution and bound to the AcChR are shown in Fig. 7 and summarized along with the molar extinction, quantum yield, and fractional change of fluorescence upon binding of each isolated monoconjugate in Table II. With the exception of the quantum yields and fractional changes of fluorescence associated with AcChR binding the spectral properties of the FITC- lys-69-, lys-35-, lys-49-, lys-23- α-toxins do not differ

greatly. The quantum yields of each of the mono-FITC derivatives are at least half of fluorescein in 0.1N NaOH (Q=0.85, Parker and Rees, 1960). The lys-69 derivative displays the highest quantum yield of the four examined, 0.41, and the lys-23 derivative the lowest at 0.18. The fractional changes in fluorescence (excitation at 480nm) associated with binding to the AcChR measured by interpolating to infinite AcChR-toxin sites (Fig. 10) showed the fluorescence of the lys 35, lys 69, and lys 49 to decrease upon binding to the receptor, 39, 26, and 6 %, respectively. In contrast, the fluorescence of the lys 23 derivative increased 96% upon binding to the receptor. When samples are radiated with 280 nm light to maximize the signal from the bound fluorophore, the spectral overlap between receptor tryptophanyl emission and fluorescein absorbance in the 520 nm band resulted in enhancement of fluorescence of FITC- lys- 23, 35, 49, and 69-toxins (data not shown).

Kinetics of isolated FITC-toxins Binding to the AcChR. As mentioned above the binding of the isolated FITC-toxins with the AcChR is associated with either decreases or increases in fluorescence. Typical recordings of the changes in fluorescence (excitation 480 nm) of FITC- lys-69-, lys-35-, lys-49-, and lys-23 -toxins upon association to the membrane-associated AcChR are shown in Fig. 8. Incubation of excess native α-toxin with AcChR before the addition of FITC-toxins showed no significant changes in fluorescence and demonstrated the ligand-specific nature of these spectral changes. The dissociation rate constants were determined by monitoring the changes in fluorescence after the addition of excess native α-toxin to a solution of FITC-toxin-AcChR complexes (Data not shown). Kinetic rate constants were derived from the slopes of plots of integrated rate expressions for bimolecular association and unimolecular dissociation (Equation 1 and 2). Examples of fits to the bimolecular association

rate expressions are shown in Fig. 8, and Table III summarizes the kinetic results. As we previously observed with the FITC-lys-23-toxin, the association kinetics of FITC- lys-35-, lys-49-, and lys-69 -toxins could be fit by a bimolecular reversible mechanism and the dissociation kinetics by a unimolecular mechanism. Within a factor of two, the average apparent bimolecular rate constants were independent of the reactant concentration ratio which ranged between 0.5 and 4. This further supports a simple reversible bimolecular inter action of the mono-FITC derivatives and the AcChR. All of the isolated mono-FITC-toxin derivatives bind to the AcChR with between 10 and 115- fold less affinity than native α-toxin. FITC-conjugation affected association more than dissociation. The association rate constants of FITC-lys -69-, -35-, -49-, and, -23 -toxins are reduced 20-, 13-, 29- and 33-fold, respectively. The dissociation rate constants were less affect by the FITC-conjugation. No more than a 5.4-fold reduction was observed (Table III).

Fig. 1. Fluorescence photograph of FITC-toxin reaction mixture and mono-FITC derivatives resolved on IPG gels. Left Panel: the photograph and optical density scan of the photograph negative of FITC-a-toxin reaction mixture (2.5 μmol α-toxin) resolved on a 5 mm thick gel. Right Panel: fluorescence photograph of isolated FITC-lys 35-toxin (Band 1; 5 nmol) , FITC- lys 69-toxin (Band 2; 5 nmol), FITC-lys 49-toxin (Band 3; 2.7 nmol), and FITC- lys 23-toxin (Band 6; 2.5 nmol) resolved on a 2 mm thick IPG gel. The isolation of the bands is described in the Experimental Procedures. Using the LKB Application Notes No. 324 the pH range of this gel was set between 9.0 and 10.0.

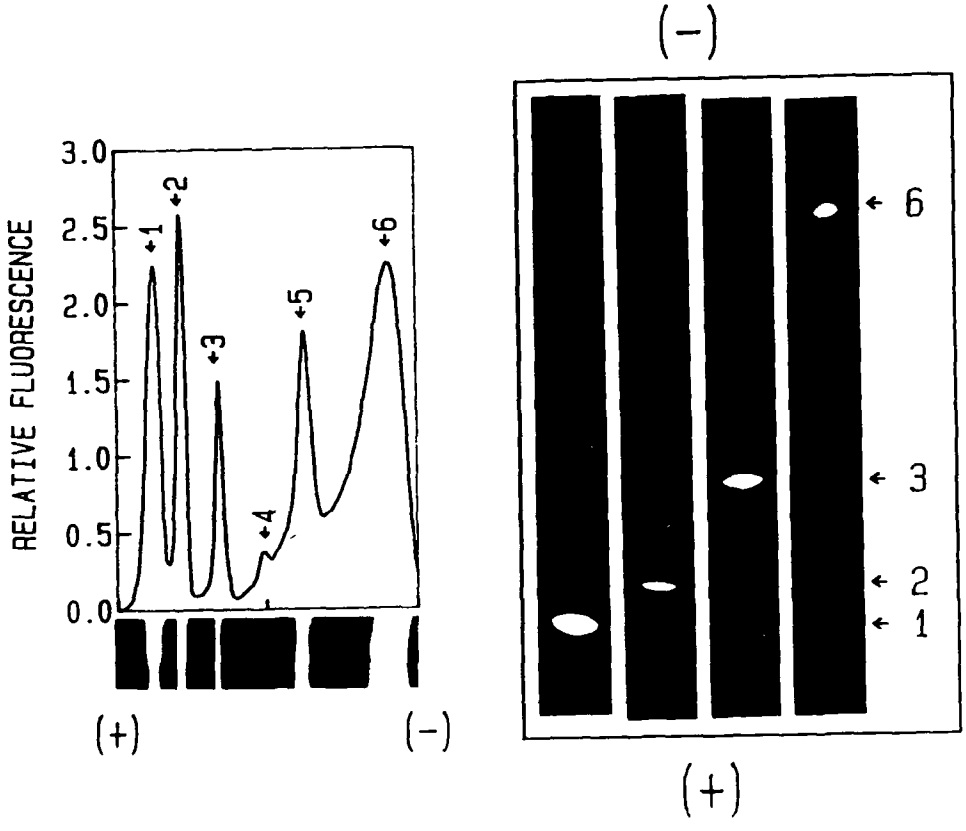

Fig. 2. HPLC elution profiles of mono-FITC derivatives extracted from the IPG gel and native α-toxin. A: Band 1; B, Band 2; C, Band 3; D, Band 6; E,native α-toxin. The peptides were resolved on a C_{18} column with a linear 80-min gradient of 20 to 40% acetonitrile against 0.1% (w/v) TFA in H_2O. Panels A-D show the elution pattern of FITC fluorescence (ex: 480; em: 520 nm). Because fluorescein does not fluoresce in low pH, aliquots (20 μl) of the fractions were mixed with 100 mM $NaPO_4$, pH 7.4, to raise the pH. Panel E shows the elution profile of α-toxin monitored at 280 nm.

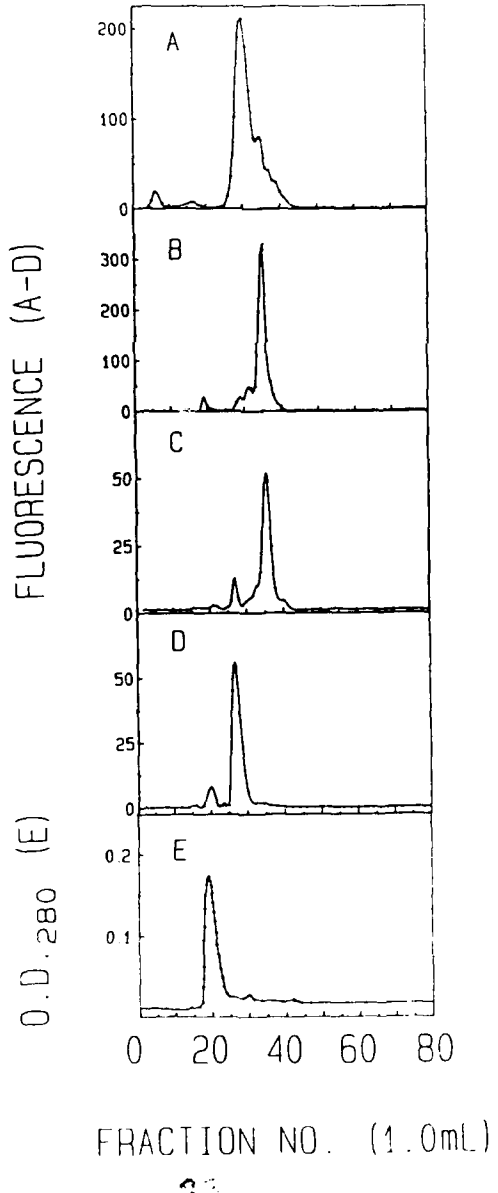

Fig. 3. HPLC elution profile of the thermolysin digestion of the Band 1,FITC-toxin monoconjugate extracted from the IPG gel described in Fig. 1. Upper Panel, peptide map of total digest resolved on a C_{18} column (0-40% acetonitrile); Lower Panel, resolution of the major peak of fluorescence peak shown in the upper panel on a C_4 column (20-35% acetonitrile); Solid line, 219nm extinction; dotted line, relative fluorescence. Elution was accomplished with specified gradients formed with acetonitrile and 0.1% TFA in H20 as given in the "Experimental Procedures."

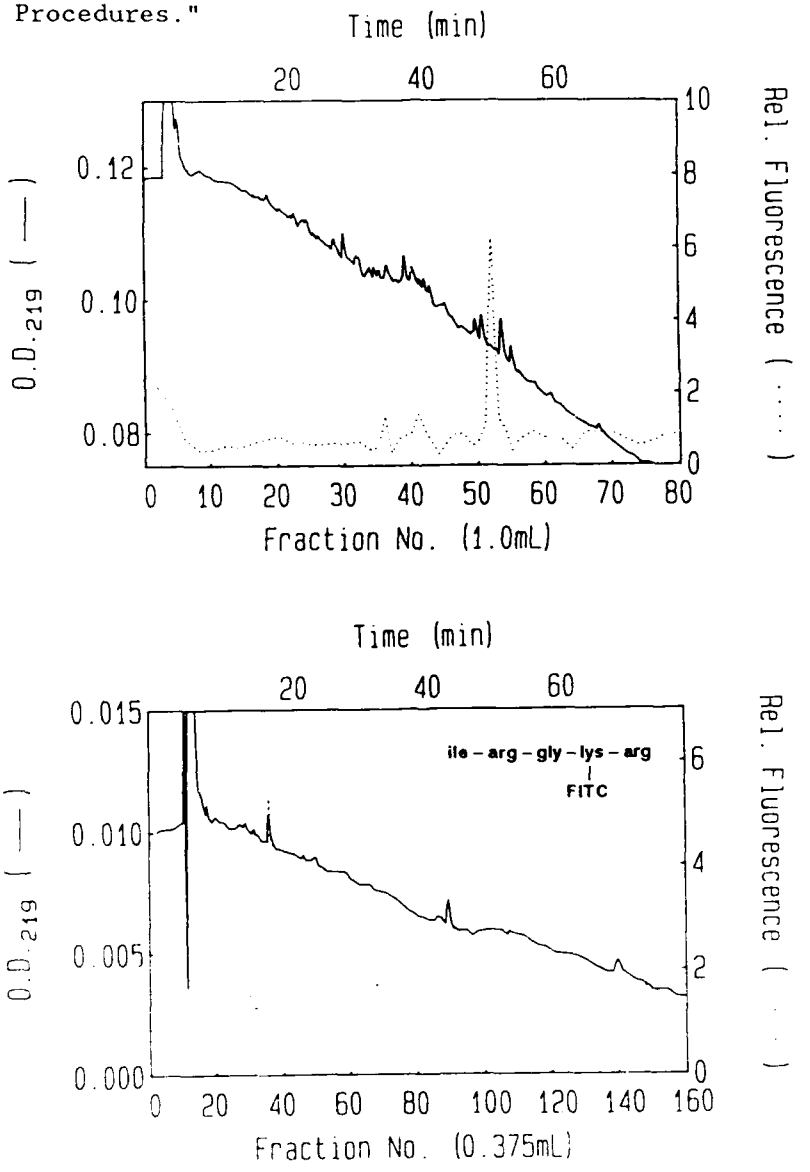

Fig. 4. HPLC elution profiles of the thermolysin digestion of Band 2 FITC-toxin monoconjugate extracted from the IPG gel described in Fig. 1. Peptide map of total digest resolved on a C_{18} column (0-40% acetonitrile). Solid line, 219nm extinction; dotted line, relative fluorescence. Elution was accomplished with specified gradients formed from acetonitrile and 0.1% TFA in H_2O as given in the "Experimental Procedures."

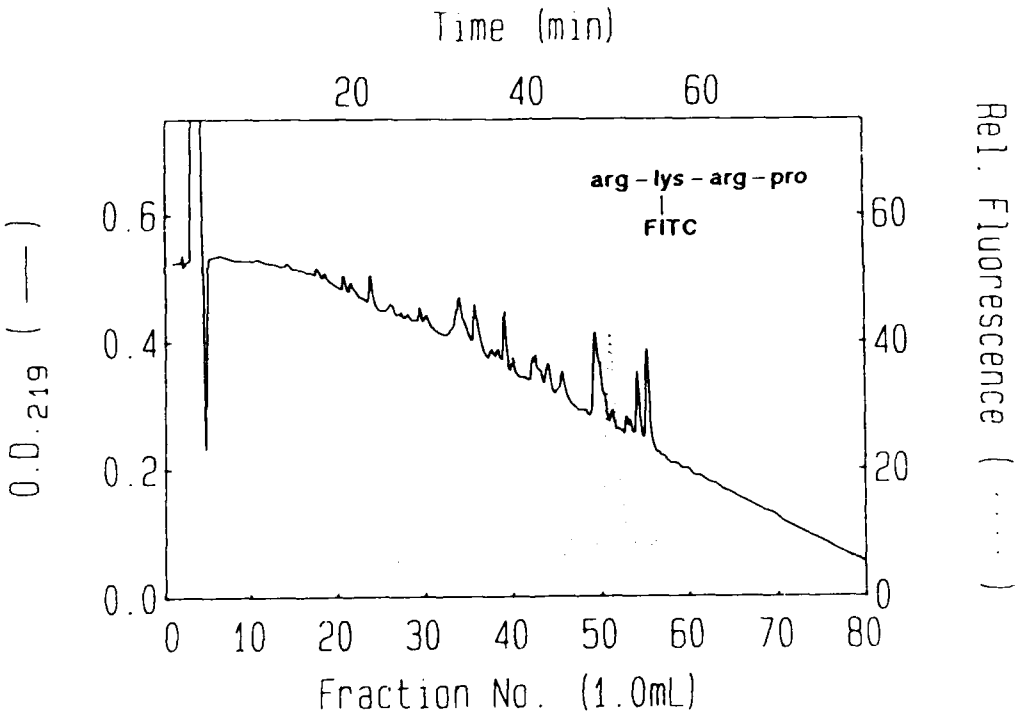

Fig. 5. HPLC elution profiles of the thermolysin digestion of Band 3 FITC-toxin monoconjugate extracted from the IPG gel described in Fig. 1. Upper Panel, total digest resolved on C_{18} column (0-40% acetonitrile). Lower Panel, major fluorescent peak in upper panel resolved on a C_4 column (20-35% acetonitrile). Solid line, 219nm extinction; dashed line, relative fluorescence. Elution was accomplished with specified gradients formed with acetonitrile and 0.1% TFA in H_2O as given in the "Experimental Procedures."

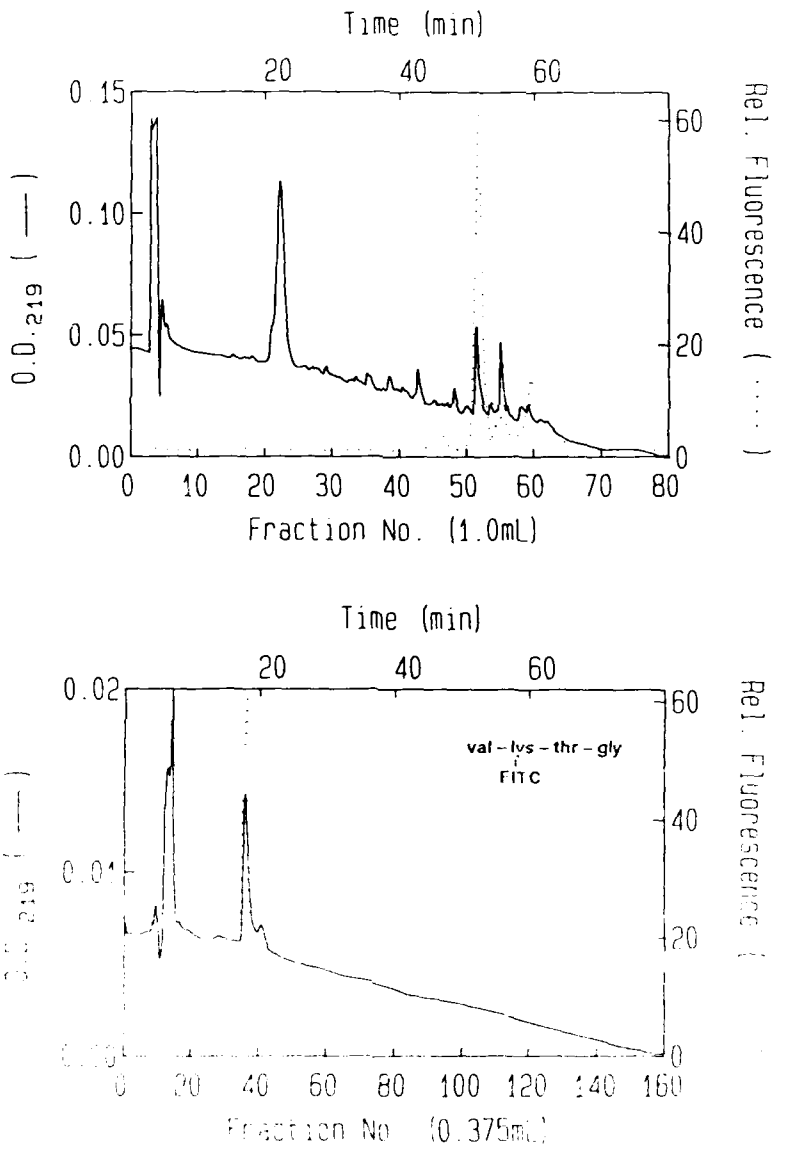

Fig. 6. Sequence of Naja naja siamensis α-toxin 3. Arrows mark sites of labeling.

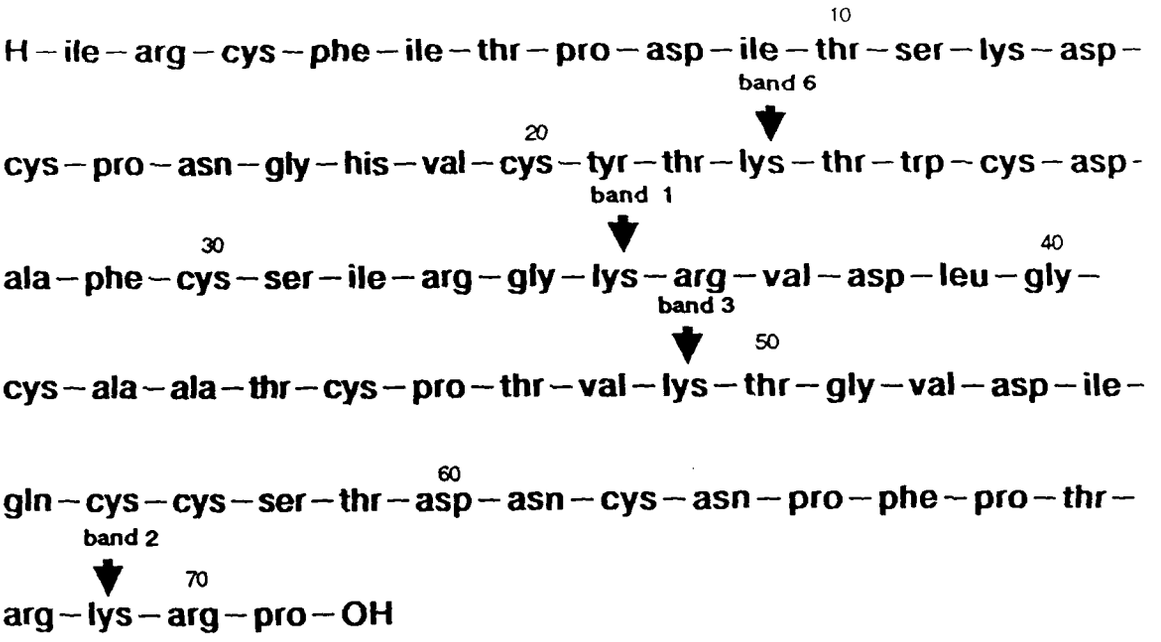

Fig. 7. The extinction (solid line) and fluorescence emission (excitation at 450 nm) spectra of the mono-FITC derivatives in the presence (dashed line)and absence (dotted line) of membrane-associated AcChR (100 nM in α-toxin sites). Panel A, FITC-lys-35-toxin; Panel B, FITC-lys-69-toxin; Panel C, FITC-lys-49-toxin; Panel D, FITC-lys-23-toxin.

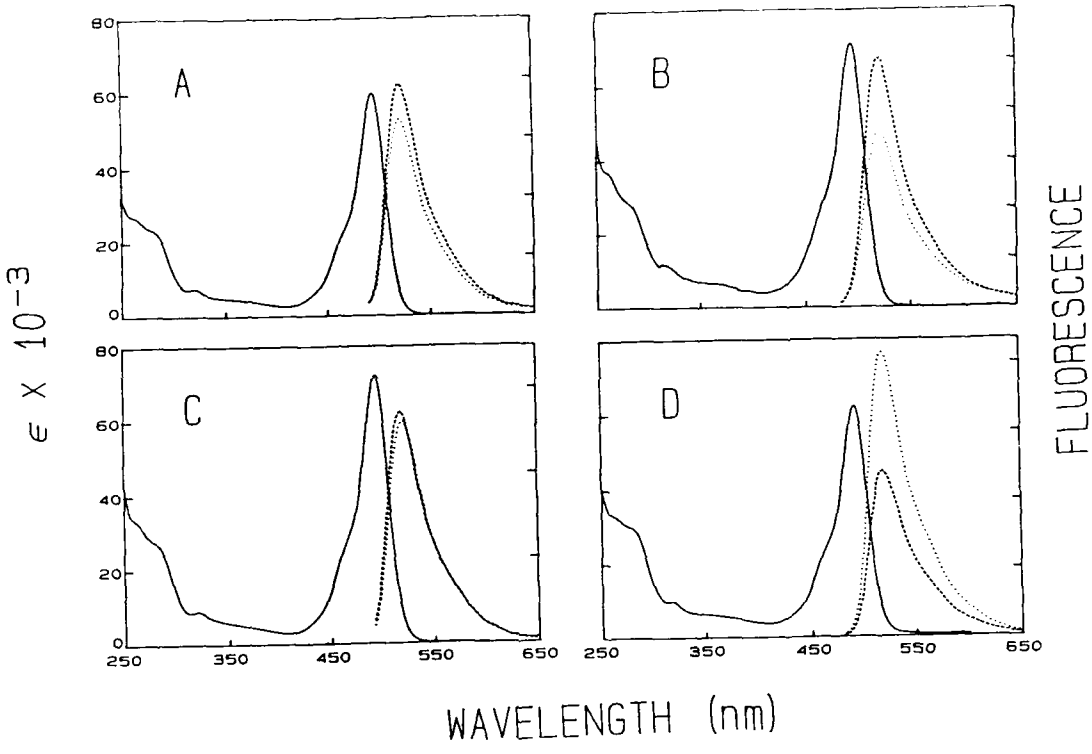

Fig. 8. The association of mono-FITC derivatives (20 nM) with the AcChR toxin sites (80 nM in a-toxin sites). Shown are the binding-dependent changes in fluorescence (excitation at 480nm, emission at 520 nm). Procedures used for detection of fluorescence are given in the Experimental Procedures. Control rates are measured in the presence of 100nM native a-toxin. Panel A, FITC-lys-35-toxin; Panel B, FITC-lys-69-toxin; Panel C, FITC-lys-49-toxin; Panel D, FITC-lys-23-toxin.

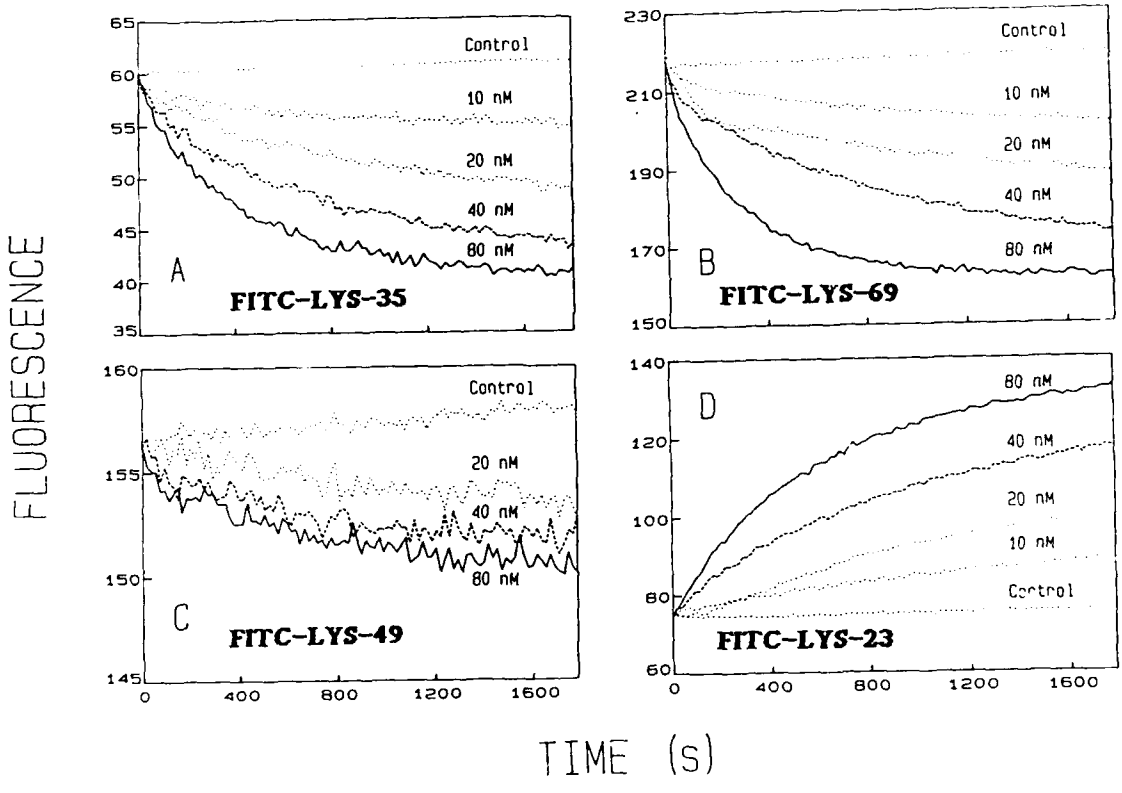

Fig. 9. Integrated rate plots of the binding (20nM FITC-toxin and 40nM AcChR in α-toxin sites) reaction fit to reversible bimolecular association mechanism (Equation 1). Panel A, FITC-lys-35-toxin; Panel B, FITC-lys-69-toxin; Panel C, Panel D, FITC-lys-49-toxin; FITC-lys-23-toxin.

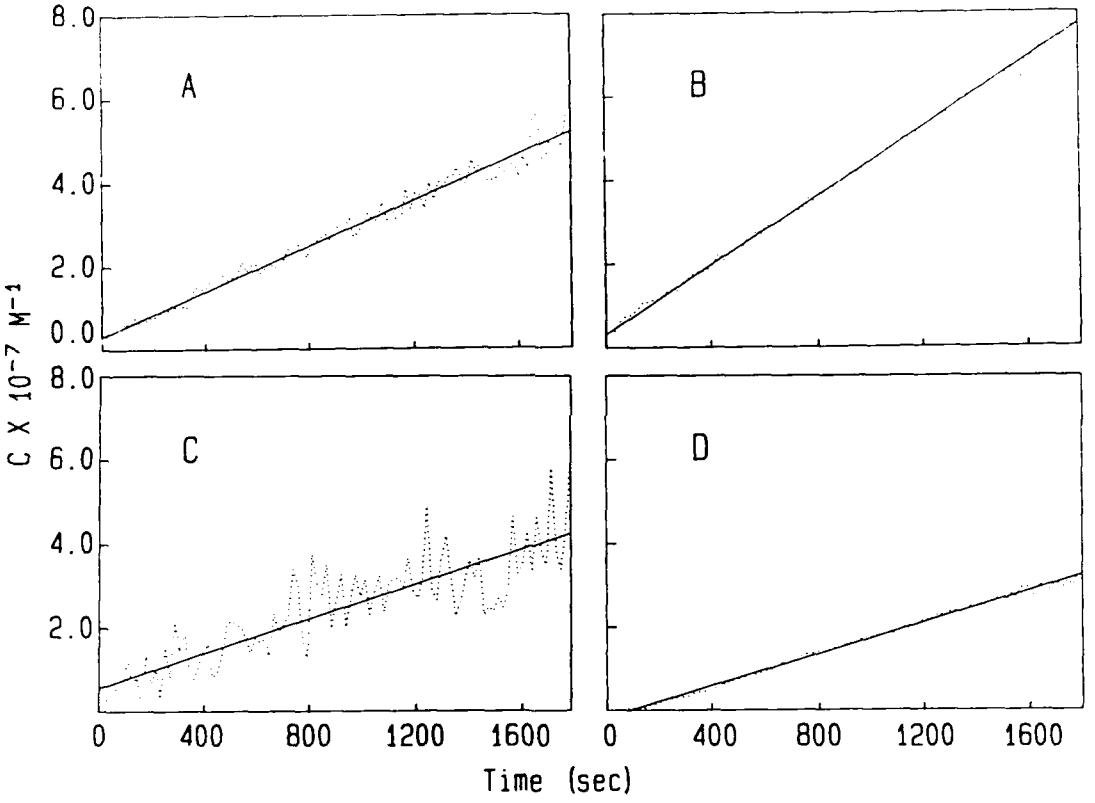

Fig. 10. Determination of the ratio of fluorescence intensity for free and bound species. Plot of the ratio of fluorescence of FITC-Toxin monoconjugates (20 nM) at equilibrium (I_e) with AcChR and free in solution (I_f) as a function of 1/[AcChR α-toxin sites]. Panel A, FITC-lys-35-toxin; Panel B, FITC-lys-69-toxin; Panel C, FITC-lys-49-toxin; Panel D, FITC-lys-23-toxin.

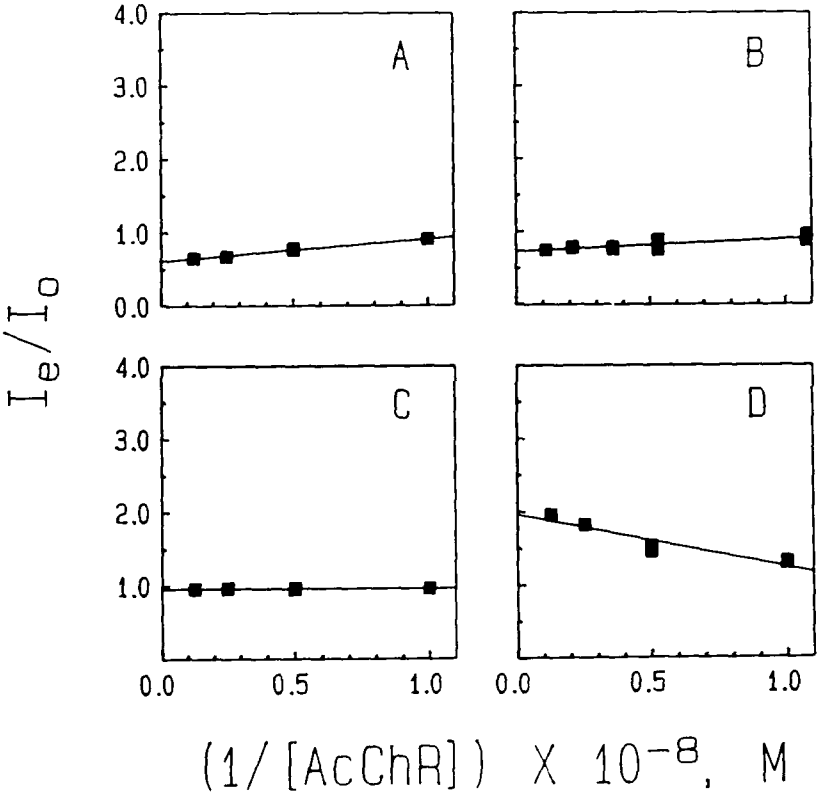

TABLE I

Effect of citraconic anhydride treatment on FITC labelling of α-toxin.

Values represent fractional estimates of mono-FITC toxins resolved on IPG gels. Quantitation of the bands was achieved by photographing UV illuminated gels, scanning the negatives with a LKB UltroScan XL Laser Densetometer, and integrating the areas under each band. Corrected values represent correction for the quantum yield and extinction using values determined when isolated bands were suspended in 100 NaCl, 10mM NaPO4, pH 7.4. (n.d.= not detectable)

	w/ citraconic anhydride		w/o citraconic anhydride	
	Uncorrected	Corrected	Uncorrected	Corrected
Band 1	.27	.20	.11	.07
Band 2	.11	.06	.10	.05
Band 3	.04	.03	.01	.01
Band 4	>.01	--	n.d.	n.d.
Band 5	.06	.03	.06	.02
Band 6	.52	.68	.72	.85

Table II

Summary of spectral properties of mono-FITC-toxins.

	Absorbance g Max. nm	e M-1cm-1	Quantum Yield	Fluorescence g Max. (nm) free
FITC-lys-35-toxin	494	60,000	0.31	520
FITC-lys-69-toxin	495	71,000	0.41	520
FITC-lys-49-toxin	494	72,000	0.38	517
FITC-lys-23-toxin	494	62,000	0.18	519

Table III

Summary of FITC-Toxin monoconjugate kinetic rate constants of association to (k_1) and dissociation from (k_{-1}) the membrane-associated AcChR.

Rate constant values represent mean %S.D. of the least squares fits to the left-hand portion of the integrated rate equations for a reversible bimolecular reaction (Equation 1) or unimolecular dissociation (Equation 2). Numbers in parentheses are the number of determinations. (* from Weiland et al., 1977)

	k_1 $M^{-1}s^{-1}$	k_{-1} s^{-1}	k_{-1}/k_1 nM
FITC-lys-35-toxin	$2.5\pm0.5\times10^{4}$(15)	$5.4\pm3.3\times10^{-5}$(3)	2.1
FITC-lys-69-toxin	$3.9\pm1.3\times10^{4}$(7)	$0.7\pm0.3\times10^{-5}$(3)	0.2
FITC-lys-49-toxin	$1.7\pm0.8\times10^{4}$(5)	$5.3\pm2.3\times10^{-5}$(3)	3.2
FITC-lys-23-toxin	$1.5\pm0.3\times10^{4}$(12)	$3.5\pm1.8\times10^{-5}$(3)	2.3
native α-toxin*	50×10^{4}	1×10^{-5}	0.02

DISCUSSION

Snake venom α-toxins have been mono-derivatized with small molecules like acetate, carbamylate, guanidinium, (Karlson et al., 1972) biotin (Lobel et al., 1985), spin labels, and dansyl (Tsetlin et al., 1979), and the various mono-derivatives isolated by chromatography on either Whatman CM-52 or BioRex 70 ion exchange resins. The larger and hydrophobic mono-FITC and mono-tetramethylrhodamine (TRITC)-toxin derivatives, however, are only partially resolved from one another and native α-toxin on either CM-52 or BioRex 70 resins (Johnson and Taylor, 1983; Johnson et al., 1985). Recoveries of mono-FITC or mono-TRITC derivatives from BioRex 70 resin are less than 10 percent and the resolution of mono-derivatives is marginally better than on CM-52 (unpublished observations). Though we previously reported the isolation of a mono-FITC-toxin (FITC-lys-23-toxin) by chromatography on CM-52 (Johnson and Taylor, 1983), our success was largely because ~85 % of the FITC (Table I) was attached to the hyperreactive ε-amino group lysine 23.

In an effort to resolve the mono-FITC-toxin derivatives, we examined column IEF, Chromatofocusing,, and reverse phase HPLC (on C_{18}, C_4, and diphenyl columns with TFA-acetonitrile gradients), and IPG techniques. Although resolution was improved with column IEF (Johnson and Taylor, 1982), Chromatofocusing (data not shown), and reverse phase HPLC (Fig. 2), the resolution was only adequate to separate native α-toxin and to some degree FITC-lys-23-toxin from other mono-FITC derivatives (Fig. 2). Focusing in IPG, on the other hand, allows the isolation of four of the six possible mono-FITC-toxin derivatives. While we have not resolved all the possible FITC-toxin derivatives, the yields and pharmacological activity of the isolated mono-FITC-toxin derivatives are sufficient to allow their use for spectroscopic analyses of the interaction of

α-toxin with the AcChR.

Since FITC forms stable bonds to primary amino groups, we expected six mono-FITC-toxin derivatives. One from each of the five lysines, plus one from the unblocked N-terminus. With Bands 1, 2, 3, 5, and 6 composed of FITC-lys-35, -69-, -49-, and, -23 -toxins and Band 5 composed of a mixture of FITC-lys-12- and FITC-ile-1-toxins, we can account for the expected mono-FITC-toxin derivatives in Bands 1, 2, 3, 5, and 6. The composition of Band 4 could not be determined due to insufficient quantities (<0.2 nmol), and may represent a FITC-conjugate of a minor contaminant of the native α-toxin solution or an unresolvable mixture of band 4 with band 5.

Relative to native α-toxin, the four mono-fluorescein derivatives, that we isolated, displayed significant lost of affinity for receptor. FITC conjugation at lys 23, lys 35, and lys 69 resulted in about 200-300 fold reduction in affinity and FITC conjugation at lys 69 about 10-fold reduction. The magnitude of these reductions in affinity are larger than reported with other modifying reagents. Lobel et al. (1985) reported no more than a 11-fold reduction of binding activity with biotinylation of the primary amino groups of α-toxin. Why FITC derivatives display, in general, lower affinity than biotinyl derivatives is unclear. The effects of chemical modification on binding are complex (Lobel et al., 1985). The greater size and negativity of FITC compared to biotin may explain the results, though modification of lys 23 with tetramethyl- rhodamine isothiocyanate, a less negatively charged analog of FITC, results in less than a 3-fold reduction in binding affinity for the receptor (unpublished observations).

Protein purification with IPG is a new (Bjellqvuist et al., 1982) and powerful chromatographic technique. A major limitation of this technique is the limited pH range (3.8-10.5) in which samples can be focused. α-Toxin, for

example, has a pI of 10.77 and consequently migrates to the cathode without focusing. Fluorescein is sufficiently negatively charged that conjugation to α-toxin decreases the pI (9.3-9.6) of the conjugate to permit IPG focusing. The conjugation of TRITC to α-toxin, on the other hand, does not lower the pI below the upper limit of IPG (10.5) (Johnson et al., 1985). Consequently, mono-TRITC-toxins currently can not be resolved with IPG. In spite of this limitation, IPG chromatography should prove a useful approach for the resolution of mixtures of mono-conjugated peptides, in which the pIs differ by less than 0.1 pH unit.

Section II

ORIENTATION OF COBRA α-TOXIN ON THE NICOTINIC ACETYLCHOLINE RECEPTOR: FLUORESCENCE DIPOLAR ENERGY TRANSFER AND QUENCHING STUDIES

INTRODUCTION

Labeled curarimimetic toxins from the venom of elapid and hydrophid snakes have played a crucial role in the identification and characterization of AcChRs. To obtain greater structural and dynamic information on the AcChR, we previously described the preparation and characterization of four derivatives of Naja naja siamemsis 3 toxin (α-toxin), labeled with fluorescein isothiocyanate (FITC) at the ε-amino groups of Lys-23, Lys-35, Lys-49, or Lys-69 (Johnson and Taylor, 1982; Johnson and Cushman, 1987). Here, we examine: (1) the solute accessibility to the above-mentioned FITC-toxin derivatives free in solution and bound to the AcChR using fluorescence quenching techniques, (2) the relative proximity of AcChR tryptophans to each site of labeling of the AcChR-bound FITC-toxins using fluorescence dipolar energy transfer techniques, and (3) the relative distance of closest approach between the surface of the lipid membrane and each site of labeling of the AcChR-bound FITC-toxins, also, using fluorescence dipolar energy transfer techniques. From these observations and

previous work on the interaction of curarimimetic snake toxins with the AcChR, we propose an approximate orientation of the curarimimetic snake toxins on the AcChR.

EXPERIMENTAL PROCEDURES

Materials. (Please see Section I).

Receptor Isolation. (Please see Section I).

Steady State Spectroscopy. (Please see Section I).

Fluorescence Lifetime. Fluorescence lifetimes were determined by the time-correlated single-photon counting technique using an EEY scientific nanosecond fluorometer (La Jolla, CA) equipped with a high-pressure hydrogen arc lamp. Fluorescence decay rates were resolved and assessed as either single or double exponential functions by using the Marquart fitting procedure. Excitation and emission bands were selected with an Oriel 450 nm broad band and 560 nm narrow band interference filters, respectively. In addition to the chromatic filters, a Polaroid HNP'B dichroic film polarizer (Norwood, MA) was placed in the observation path and rotated at an angle of 55° from vertical to eliminate anisotropic contributions to the observed decay. Correction for light scattering was made by subtracting the decay curve of samples containing all the components except the fluorophore. The instrumental arrangement and principles of data treatment have been discussed in detail elsewhere (Yguerabide, 1972).

Solute Accessibility to Sites of Labeling on Receptor-Bound α-Toxins. Solute accessibility to FITC conjugated to α-toxin at Lys-23, Lys-35, Lys-49, or Lys-69 was assessed as the magnitude of the bimolecular quenching rate constant, k_{FQ}, for iodide. A detailed description of the theory and method are provided elsewhere (Johnson and Yguerabide, 1985). Briefly, the fluorescence intensities of the fluorophores were monitored as a function of the iodine concentration.

The intensities were then analyzed with the Stern-Volmer equation

$$I_o/I = 1 + K_Q\,[Q] \qquad (6)$$

where I_o and I are fluorescence intensities observed in the absence and presence of a concentration [Q] of iodine. K_Q, the Stern-Volmer quenching constant, was related to k_{FQ} by the equation

$$K_Q = k_{FQ}\,\tau \qquad (7)$$

where τ is the fluorescence lifetime.

Unless indicated otherwise, all samples were dissolved (at 20°C) in 1 M NaCl, 10 mM sodium phosphate buffer, pH 7.4, and sodium thiosulfate (0.1mM) to prevent formation of triiodide anion. High NaCl concentration was used to minimize surface charge effects.

Energy Transfer. The efficiency of dipolar resonance energy transfer between discrete donors and suitable acceptors is related to the distance (R) separating the two molecules by Equation 8 (Forster, 1959).

$$E = (R_o/R)/\{1 + (R_o/R)^6\} \qquad (8)$$

where R_o represents the distance at which transfer efficiency is 50% and is evaluated from the following equation.

$$R_o = 9.765 \times 10^3(\kappa^2 J Q n^{-4})^{1/6} \qquad (9)$$

The overlap integral, J, is calculated from the experimental spectra through the relationship

$$J = \Sigma I_D(\lambda)\epsilon_A(\lambda)\lambda^4\Delta\lambda / \Sigma I_D(\lambda)\Delta\lambda \qquad (10)$$

where $\epsilon_A(\lambda)$ is the molar extinction coefficient of the energy acceptor and $I_D(\lambda)$ is the donor emission spectrum. Q denotes the donor quantum yield in the absence of acceptor. n represents the refractive index of the medium between donor and acceptor. κ^2, the orientation factor, accounts for the relative orientation of the donor emission and acceptor absorption transition dipoles and is assumed here

to be equal to 0.67. λ is the wavelength in cm.

Sensitization of Acceptor Fluorescence. Where the acceptor is fluorescent, transfer efficiency can usually be estimated from measurements of either donor quenching or acceptor sensitization. In the case where excitation occurs at the donor wavelength and the emission is monitored at the acceptor wavelength, the transfer efficiency (E_A) is monitored as the sensitized acceptor emission and can be calculated with Equation 11 (Schiller, 1975).

$$E_A = A_A/A_D \ (I_{AD}/I_A - 1) \qquad (11)$$

where I_{AD} and I_A are the emission intensities of the acceptor in the presence and absence of donor, respectively. A_D and A_A are the absorbances at the excitation wavelength of the donor and acceptor, respectively.

Relative Energy Transfer Between AcChR Tryptophans and FITC Conjugated to AcChR-bound α-Toxins. Energy transfer from AcChR tryptophans to the FITC conjugated to the ε-amino groups of Lys 23, Lys 35, Lys 49, or Lys 69 on the AcChR-bound cobra α-toxin was measured as sensitized FITC emission. The relative energy transfer was quantitated as the ratio of the fluorescence of FITC-toxin AcChR-bound (I_b) and free in solution (I_f) upon excitation of the AcChR tryptophan (EX: 280 nm). Individual determinations were made by placing samples of membrane-associated AcChR (10-100 nM in α-toxin sites) in a 1 cm quartz cuvette and measuring the apparent fluorescence to determine the background fluorescence. After the background fluorescence was determined, 20 nM of FITC-toxin was added and the time-dependent change in fluorescence was monitored as the FITC-derivatives bound to the AcChR. Background fluorescence was subtracted from each datum point. The first data sampling after the addition of the FITC-toxin defined the fluorescence of the free FITC-toxin (I_f) and interpolation of the a double-reciprocal plot of fluorescence versus time to

infinite time yielded the equilibrium fluorescence (I_e). Because the quantum yields of the derivatives change upon binding, the observed I_b/I_f ratios were divided by the previously determined intrinsic binding-dependent changes in FITC-toxin fluorescence (Johnson and Cushman, 1988). All samples were dissolved in 100 mM NaCl, 10 mM sodium phosphate, at pH 7.4 at 20°C.

Distance of Closest Approach Between the Lipid-Membrane Surface and the Sites of Labeling on the AcChR-Bound FITC-toxins. The capacity of the various AcChR-bound FITC-toxins to transfer energy to C_{12}-eosin, incorporated into the lipid-membrane surface, was used to assess the relative distance of closest approach between the lipid-membrane surface and the sites of labeling of AcChR-bound FITC-toxins. The FITC-toxins (50 nM) were incubated with membrane-associated AcChR (100 nM in α-toxin sites) for 90 min before the start of the C_{12}-eosin (200 μM in DMSO) titration. Nonspecific energy transfer was estimated by titration of C_{12}-eosin into samples in which the FITC-toxins were prevented from binding to the AcChR by prior incubation of excess native α-toxin (2.5 μM). Background and fluorescence from directly excited C_{12}-eosin, were estimated from the titration of C_{12}-eosin into samples containing all the components except the FITC-toxins. Titrations were performed in 0.5 cm cuvettes excited at 450 nm and monitored at 510 nm. To reduce stray light effects Oriel 450 nm broad band interference and a Corning 3-70 cut-off filters were placed in the paths of excitation and emission beams, respectively. Energy transfer was measured as the extent of donor quenching after background and C_{12}-eosin fluorescence was subtracted.

To obtain a relative estimate of distance of closest approach between the lipid membrane surface and each site of derivatization of the AcChR-bound FITC-toxins, the plots of Q_D/Q_{D_A} versus σR_o^2 were fit to Equation 12 (Shaklai et al.,

1977; Holowka and Baird, 1983b).

$$Q_D/Q_{DA} = 1 + (\pi R_o^6/2)(1/L)^4\sigma \qquad (12)$$

where Q_D is the donor fluorescence in the absence of the C_{12}-eosin and L is the distance of closest approach between donors and acceptors. σ represents the surface density (no. of acceptors/unit area). Equation 12 assumes a model in which donors are randomly distributed in a plane at a fixed distance, L, away form a plane of acceptors at the lipid membrane surface. The model also assumes κ^2 equals 2/3 and $L > 1.68R_o$.

Probe Surface Density. The surface density of acceptor probes, σR_o^2, was determined by the energy transfer method of Holowka and Baird (1983a). Briefly, C_{12}-eosin was titrated into samples of AcChR-enriched membranes (100nM in α-toxin sites), containing 5-(dodecanoylamino)-fluorescein (100nM), while monitoring the fluorescein fluorescence (EX: 450nm; EM: 510nm) in the absence (Q_D) and presence (Q_{DA}) of C_{12}-eosin. A best fit to a curve generated from Equations 13 and 14 (Wolber and Hudson, 1979), which assume distances of closest approach of $0.0R_o$ and $0.25R_o$, respectively, was used to relate the observed Q_D/Q_{DA} ratios to σR_o^2.

$$Q_{DA}/Q_D = 0.6463 \exp(-4.7497\sigma R_o^2) + 0.3537 \exp(-2.0618\sigma R_o^2) \qquad (13)$$

$$Q_{DA}/Q_D = 0.6290 \exp(-4.5752\sigma R_o^2) + 0.3710 \exp(-1.9955\sigma R_o^2) \qquad (14)$$

RESULTS

Solute Accessibility. The bimolecular quenching rate constant, k_{FQ}, is the fundamental parameter for the evaluation of solute accessibility. Determination of the bimolecular quenching constant requires the measurement of both the fluorescence lifetime and the Stern-Volmer quenching constant, K_Q, (Equation 7). The monoexponential fluorescence decay of FITC-Lys-35, -Lys-69, and -Lys-49 α-toxin free in solution or bound to the membrane-associated AcChR are shown in

Fig. 11 and the lifetimes summarized in Table IV. We have previously reported the fluorescence lifetime of FITC-Lys-23-toxin (Johnson and Yguerabide, 1985). The binding of the FITC-toxins to the AcChR had little affect on the decay rates. The Stern-Volmer plots for iodide quenching of the fluorescein, the FITC-toxins in the presence of native α-toxin bound to the AcChR, and the FITC-toxin derivatives bound to the acetylcholine receptor are shown in Fig. 12 and Table IV summarizes the calculated K_Qs from linear least squares fits to these plots. Over the concentration range examined, all the Stern-Volmer quenching plots were linear. Using Equation 7 and the measured lifetimes, the bimolecular quenching rate constants were calculated and summarized in Table IV. The bimolecular quenching rate constants of the fluorescein moiety of the derivatives were reduced by about the same extent both upon conjugation to the α-toxin (50 to 57%) and following binding of the conjugate to the AcChR (62 to 67% relative the free fluorescein). These results show, that both upon conjugation to the α-toxin and binding of the FITC-toxins to the AcChR, the fluorescein moiety of each FITC-toxin were equally accessible to the bulk solute. Since the changes in the rotational motion of the FITC associated with conjugation and the binding of the conjugate to the receptor would reduce the bimolecular quenching rate constants by about 60%, (Johnson and Yguerabide, 1985), these results suggest that the FITC moieties of each derivative examined are completely exposed to the iodide ion even after binding to the AcChR.

Dipolar Energy Transfer Between Receptor Tryptophans and FITC-toxins. Since the AcChR contains 53 tryptophan residues, mostly (42) distributed throughout the extracellular domains (residues 1-210) of the 5 subunits of the AcChR (α, 11x2 tryptophans; β, 10; γ, 11; δ, 10) (Noda et al, 1982; Noda et al., 1983; Claudio et al., 1983), it may be reasonable to utilize the energy transfer

to estimate the relative distance between the FITC moiety on the bound-toxin derivatives and the surface of the receptor. We measured the magnitude of energy transfer as the sensitized enhancement of fluorescence upon binding. Figs. 3A-D show the fluorescence of each of the FITC-toxins increase upon binding. The magnitude of the enhancement of fluorescence (I_b/I_f) was determined by interpolating plots of bound equilibrium over the initial fluorescence (I_e/I_o) versus the reciprocal concentration of AcChR to infinite receptor concentration (Figs. 4A-D). Table V summarizes these results. The observed fluorescence of the FITC-Lys-23-, -Lys-35-, -Lys-49-, and -Lys-69-toxins increased upon binding 430, 120, 150, and 300%, respectively, Since the quantum yield of the FITC-toxins differentially change upon binding (Johnson and Cushman, 1988), the observed binding-enhancements of fluorescence were corrected for intrinsic changes in fluorescence. Corrected for intrinsic enhancements of fluorescence, the Lys 49 displayed the greatest increase upon binding (310%), while the Lys 23, Lys 35, and Lys 69 derivatives displayed about the same magnitude increase (218, 201, and 210%, respectively) (Table V). These results suggest that, on the AcChR-bound toxin, the Lys 49 site is closer to the AcChR than Lys 23, Lys 35, or Lys 69, which are about equidistance from the receptor.

Dipolar Energy Transfer Between the Lipid-Membrane Surface and Sites of FITC labeling on AcChR-Bound α-Toxins. The spectral relationship for the donor FITC-Lys-23-toxin and C_{12}-eosin is shown in Fig. 15 and the calculated overlap integrals of the FITC-toxins and C_{12}-eosin are presented in Table VI. In the calculation of the overlap integral, the excitation spectra of the membrane-associated C_{12}-eosin (assuming a maximum molar extinction of 8.5×10^4 $M^{-1}cm^{-1}$) was utilized to estimate the absorption spectra of the membrane-associated C_{12}-eosin, because light scatter from AcChR-enriched membranes interfered with absorption

measurements. Only the FITC-Lys-23-toxin spectra are shown because of the great similarity to the other FITC-toxins studied (Johnson and Cushman, 1988). The Forster critical distances, R_o, between the AcChR-bound FITC-toxins and C_{12}-eosin ranged between 41.6 and 45.8 Å (Table VI).

Fluorescence of the fluorescein moieties of the FITC-toxins and 5-(N-dodecanoylamino)-fluorescein in the presence of AcChR-enriched membrane fragments was diminished upon addition of C_{12}-eosin. The plots (Q_D/Q_{DA} versus [C_{12}-eosin]) of the titration of C_{12}-eosin into samples containing the FITC-toxins free in solution and AcChR-bound and the 5-(N-dodecanoylamino)-fluorescein partitioned into AcChR-enriched membrane fragments are shown in Fig. 16. The magnitude of quenching of FITC-toxins free in solution was subtracted from AcChR-bound FITC-toxins to obtain the magnitude of specific quenching. The relative distances of closest approach were then calculated from the slopes of plots the specific quenching of the FITC-toxins as a function of the surface density (σR_o^2) of C_{12}-eosin and Equation 12 (Fig. 17). The Lys 23 on the AcChR-bound α-toxin is the closest (40 Å) to the lipid membrane surface followed by Lys 49 (41 Å), Lys 35 (45 Å), and Lys 69 (46 Å).

Fig. 11. Nanosecond fluorescence decay curves of FITC-Lys-35-toxin, FITC-Lys-69-toxin, and FITC-Lys-49-toxin bound to the AcChR and free in solution. (A and B) FITC-Lys-35-toxin; (C and D) FITC-Lys-69-toxin; (E and F) FITC-Lys-45-toxin. (A, C, and E) The FITC derivatives (0.4 μM) were bound the AcChR (0.6μM in α-toxin sites), and (B, D, and F) free in solution in the presence of native α-toxin bound AcChR. Dashed lines represent the lamp pulse. Deviation of the experimental (dotted) from single exponential theoretical (solid) function are shown in the curves above each decay plot.

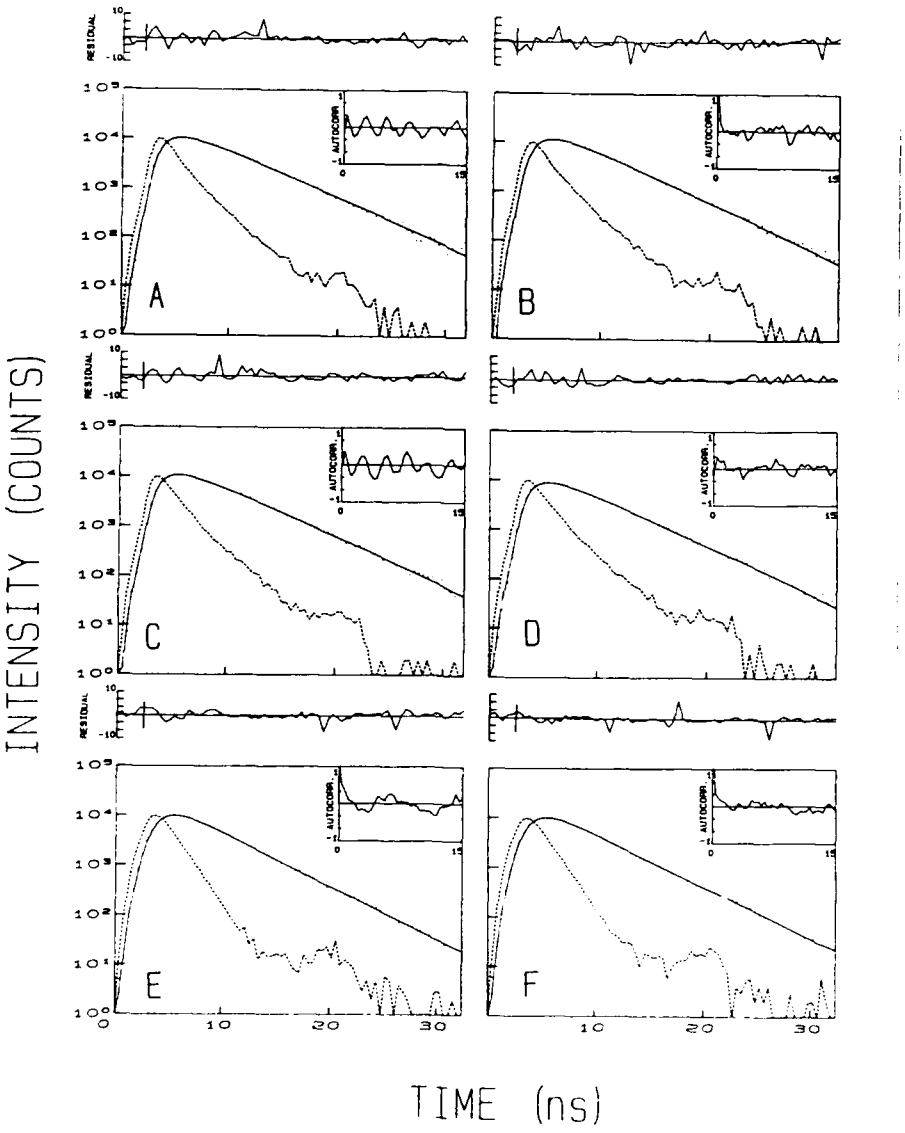

Fig. 12. Stern-Volmer plots of iodide quenching of the fluorescence of fluorescein (filled circles), FITC-toxin bound to the AcChR (filled squares), and FITC-toxin free in a solution containing native α-toxin-saturated AcChR (open squares). Panel A, FITC-Lys-35-toxin; Panel B, FITC-Lys-69-toxin; Panel C, FITC-Lys-49-toxin; Panel D, FITC-Lys-23-toxin.

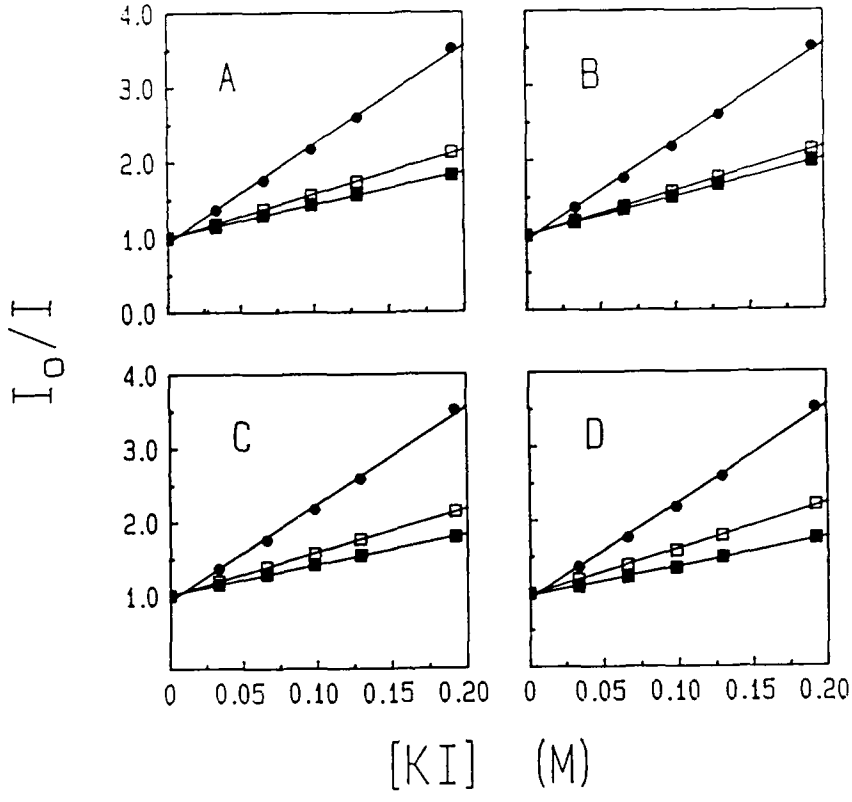

Fig. 13. The association of mono-FITC derivatives (20 nM) with the AcChR toxin sites (80 nM in α-toxin sites). Shown are the binding-dependent changes in fluorescence (EX: 280nm; EM: 520 nm). Procedures used for detection of fluorescence are given in the Experimental Procedures. Panel A, FITC-Lys-35-toxin; Panel B, FITC-Lys-69-toxin; Panel C, FITC-Lys-49-toxin; Panel D, FITC-Lys-23-toxin.

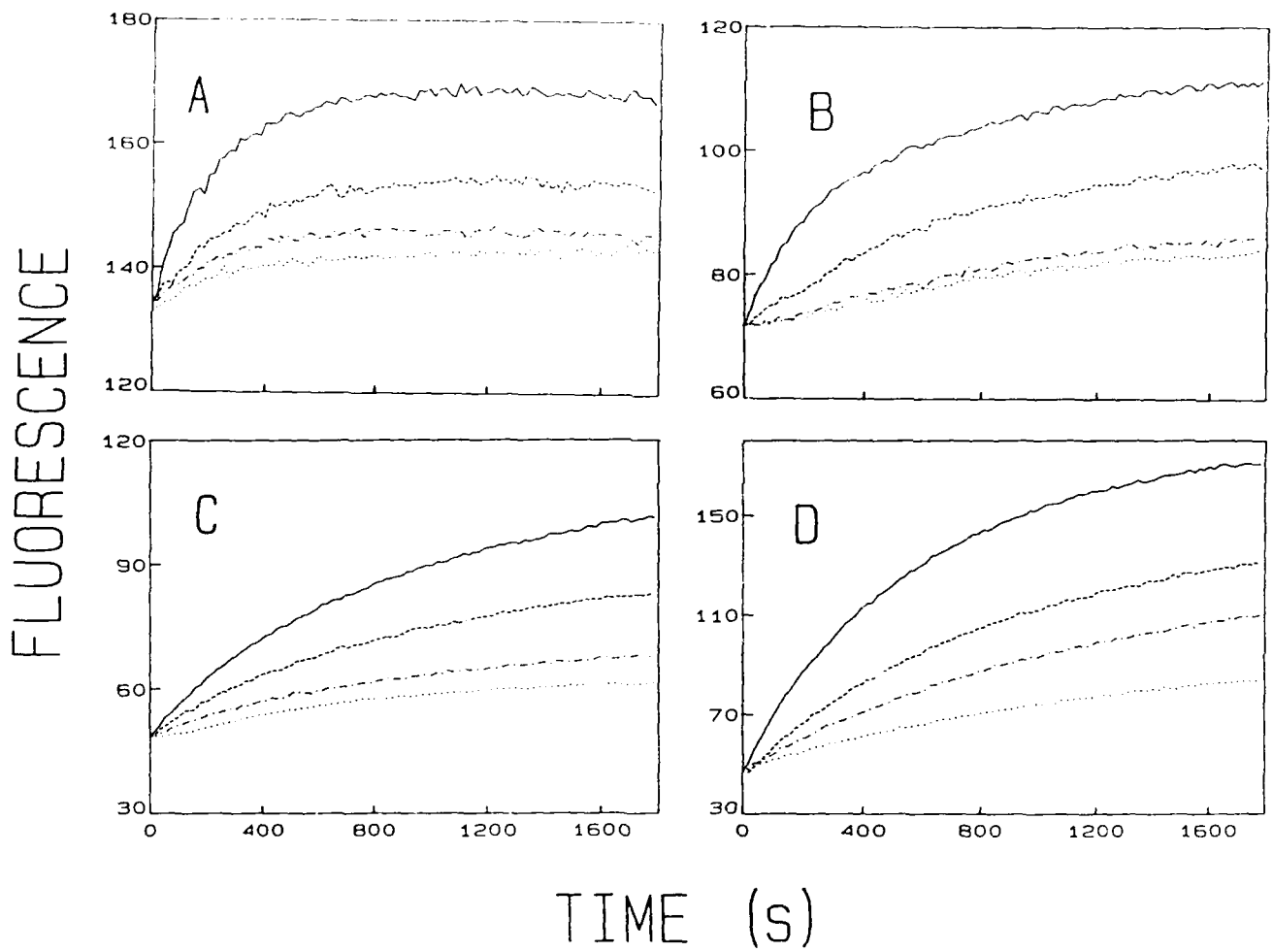

Fig. 14. Determination of the ratio of fluorescence intensity for free and bound species. Plot of the ratio of fluorescence of FITC-toxin monoconjugates (20 nM) at equilibrium (I_e) with AcChR and free in solution (I_f) as a function of 1/[AcChR α-toxin sites]. Panel A, FITC-Lys-35-toxin; Panel B, FITC-Lys-69-toxin; Panel C, FITC-Lys-49-toxin; Panel D, FITC-Lys-23-toxin.

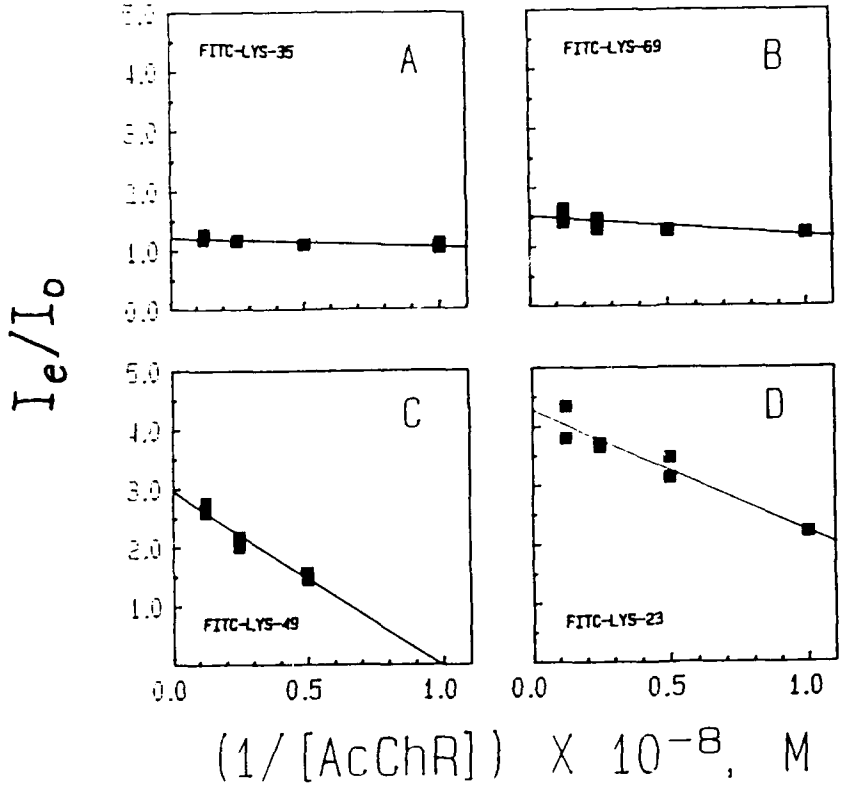

Fig. 15. Spectral overlap of donor AcChR-bound FITC-Lys-23-toxin and acceptor C_{12}-eosin. Shown are the absorption spectrum of FITC-Lys-23-toxin in buffer (----), corrected excitation spectrum of C_{12}-eosin partitioned into AcChR-enriched membrane fragments (····), and the corrected emission spectra of AcChR-bound FITC-Lys-23-toxin (–·–·–) and C_{12}-eosin (0.44μM) partitioned into AcChR-enriched membranes (——)(100nM in α-toxin sites).

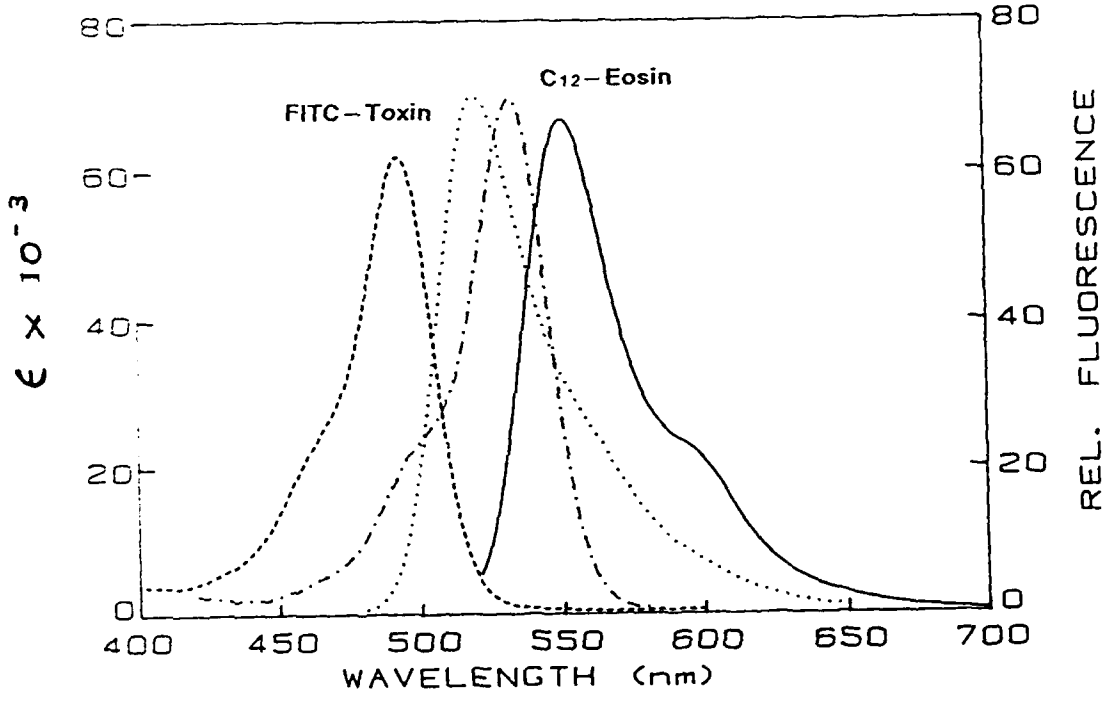

Fig. 16. Titration of acceptor C_{12}-eosin into AcChR-enriched membrane fragments (100nM in α-toxin sites) with FITC-toxins (50nM) bound (filled circles) or prevented from binding by prior incubation with excess (2.5 μM) native α-toxin (open circles) (EX:450; EM:510nm). Open boxes represent AcChR membrane fragments (100nM in α-toxin sites) and 5-(N-dodecanoylamino)fluorescein. Plotted are the ratios of donor quantum yield in the absence (Q_D) and presence (Q_{DA}) of acceptor C_{12}-eosin as a function of the concentration of added C_{12}-eosin. Panel A, FITC-lys-23-toxin; Panel B, FITC-lys-35-toxin; Panel C, FITC-lys-49-toxin; Panel D, FITC-lys-69-toxin.

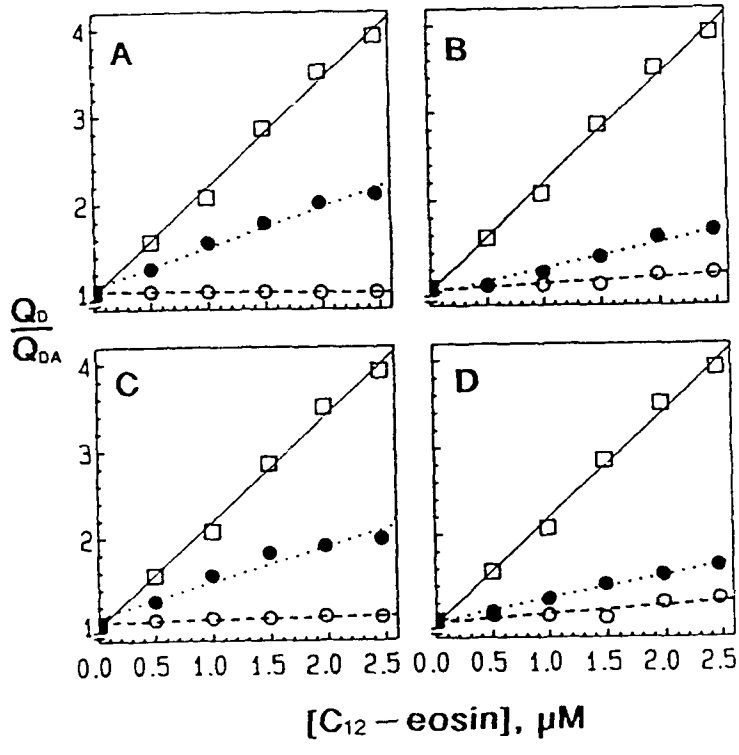

Fig. 17. Energy transfer between AcChR-bound FITC-toxins and acceptor C_{12}-eosin at the lipid-membrane surface. The fluorescence was corrected by subtraction of the signal from samples in which FITC-toxins were prevented from binding to the AcChR with prior incubation with excess native α-toxin). The ratio of donor quantum yield in the absence (Q_D) and presence (Q_{DA}) of acceptor C_{12}-eosin is plotted as a function of acceptor density. Panel A, FITC-lys-23-toxin; Panel B, FITC-lys-35-toxin; Panel C, FITC-lys-49-toxin; Panel D, FITC-lys-69-toxin.

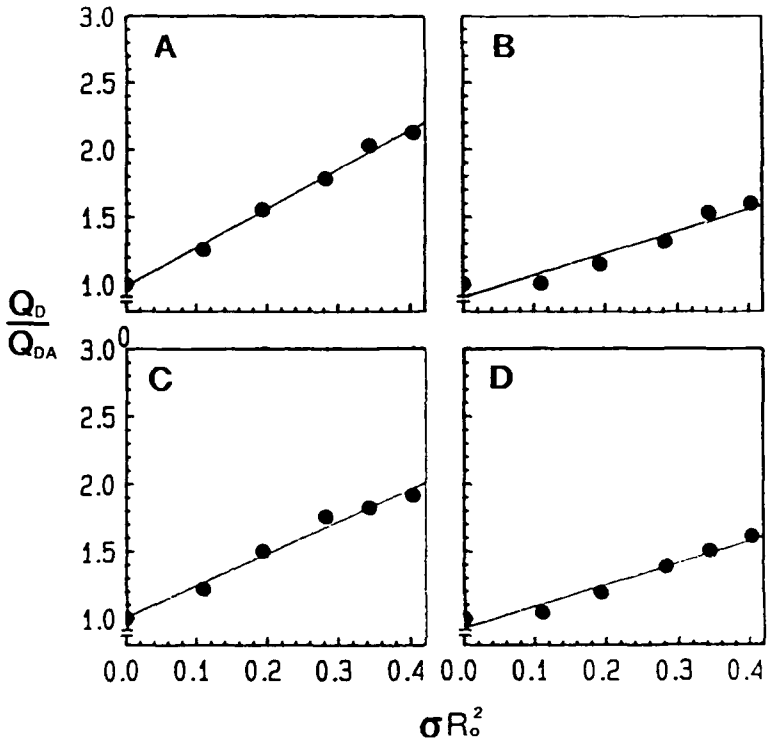

Fig. 18. Model of the orientation of α-toxin bound to the extracellular protrusion of the AcChR. The ellipsoidal shaped α-toxin (concave surface on shown) sits on the apical extracellular surface of the receptor with the major axis of the α-toxin titling from a perpendicular membrane projection. The various sites of FITC labeling are shown approximately as smaller-numbered spheroids and are based on the x-ray coordinates of native α-toxin (Walkinshaw et al., 1980).

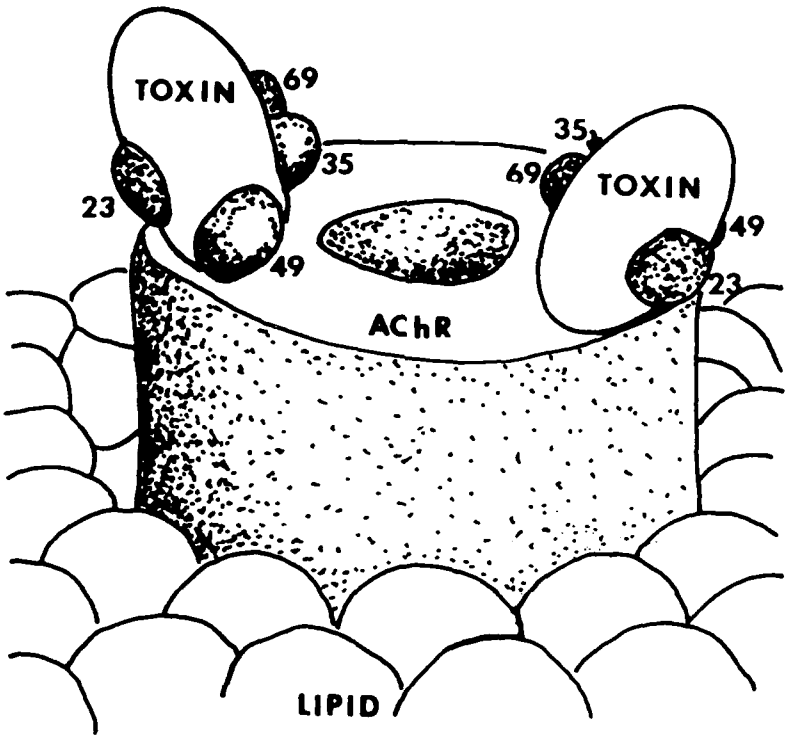

Table IV

Summary of the Stern-Volmer Plots and fluorescence decay rates of FITC-toxins and fluorescein free in solution and AcChR-bound

	Lifetime (ns)		K_Q[a] (M)		$k_Q \times 10^{-9}$[b] ($M^{-1}s^{-1}$)		k_{FITC}/k_{fl}[c]	
	free	bound	free	bound	free	bound	free	bound
FITC-Lys-23-toxin	3.9[d]	3.81[d]	6.3±0.1	4.0±0.1	1.60±0.02	1.04±0.05	0.50	0.33
FITC-Lys-35-toxin	4.2	4.1	5.9±0.2	4.3±0.1	1.40±0.05	1.05±0.02	0.44	0.33
FITC-Lys-49-toxin	3.8	3.9	6.0±0.1	4.1±0.1	1.57±0.02	1.06±0.02	0.49	0.33
FITC-Lys-69-toxin	4.3	4.1	5.9±0.2	5.0±0.2	1.37±0.05	1.22±0.05	0.43	0.38
free fluorescein	4.1		13.1±0.2		3.19±0.04			

[a]Stern-Volmer quenching constant. [b]Bimolecular quenching constant calculated using Equation 7. [c]k_{FITC}/k_{fl} represent the ratio of each FITC-toxin to fluorescein bimolecular quenching constants. [d]From Johnson and Yguerabide, 1985.

Table V

Comparison of the effect of excitation at 280 versus 480nm on the change FITC-toxin steady-state fluorescence associated with the binding to the AcChR.

	I_b/I_f		
	Ex:280nm	Ex:480nm[a]	Ex:280/Ex:480[b]
FITC-Lys-23-toxin	4.28±0.12	1.95±0.68	2.18
FITC-Lys-35-toxin	1.22±0.03	0.61±0.01	2.01
FITC-Lys-49-toxin	2.97±0.13	0.95±0.01	3.11
FITC-Lys-69-toxin	1.52±0.05	0.73±0.03	2.10

[a]Values from Johnson and Cushman (1988). [b]Ratio of the binding-dependent changes in fluorescence with excitation at 280nm to 480nm.

Iodine titrations were performed in 1 cm^2-cross-section cuvettes maintained at 20°C. Samples were excited at 480 nm, and the emission was monitored at 520 nm with a Corning 3-69 filter in the path of the emission beam. Fluorescence values were corrected for dilution resulting from added titrant and background fluorescence.

Table VI

Summary of Energy Transfer Parameters for donor fluorescein derivatives and acceptor, C_{12}-eosin.

Donor	Q[a]	Acceptor	ϵ_A[d]	J[e]	R_o[f]	K[g]	R[h]
			($M^{-1}cm^{-1}$)	cm^6 mol	Å	$x10^{-5}$ M	Å
FITC-Lys-23-toxin	0.35[b]	C_{12}-eosin	85,000[c]	$2.94x10^{-13}$	45.8	4.7±03	40
FITC-Lys-35-toxin	0.19[b]	C_{12}-eosin	85,000[c]	$3.09x10^{-13}$	41.6	2.2±0.3	45
FITC-Lys-49-toxin	0.36[b]	C_{12}-eosin	85,000[c]	$3.16x10^{-13}$	46.4	3.8±0.5	41
FITC-Lys-69-toxin	0.30[b]	C_{12}-eosin	85,000[c]	$3.13x10^{-13}$	45.1	1.7±0.1	46
5-(dodecanoylamino) fluorescein	0.34[c]	C_{12}-eosin	85,000[c]	$3.03x10^{-13}$[c]	50.1[c]	12.2±0.5	

[a]Quantum yield. [b]Q_D was calculated by multiplying the quantum yield of the free derivative by the fractional change of fluorescence with direct excitation (Ex: 480 nm) upon binding from data determined elsewhere (Johnson and Cushman, 1988). [c]Values from Holowka and Baird (1983a). [d]Molar extinction at maximum visible wavelength. [e]Overlap integral defined by Equation 10. [f]Forster critical distance defined by Equation 9 (assumptions: $\kappa^2 = 2/3$ and n=1.6). [g]K, specific slope of Q_D/Q_{DA} versus C_{12}-eosin plots in Fig. 15. [h]Calculated distance of closest approach between C12-eosin on the surface of the lipid membrane and the site of FITC derivatization on the AcChR-bound α-toxin using Equation 12.

DISCUSSION

Curarimimetic snake toxins are polypeptides, falling into one of two structural classes based on the number of residues, short (60-62 residues) and long (71-74 residues) toxins (Dufton and Hider, 1983). The crystal structures of a short (Low et al, 1976; Tsernoglou and Petsko, 1976) and two long toxins (Walkinshaw et al., 1980; Agard and Stroud, 1982) reveal common features: three roughly parallel loops emerging from a globular head. The main or central loop (residues 21-40, relative to the siamensis 3 toxin) is flanked on either side by two shorter loops (residues 4-13 and 44-55). In long toxins, a flexible C-terminal tail (63-71) hangs down behind the central loop. Diagrammatically, curarimimetic snake toxins can be described as concave ellipsoids 40x30x20 Å. The Lys 23 residue is situated near the center of the concave surface of the ellipsoid. Lys 35 and Lys 69 are situated near one another on the center of the convex surface, and Lys 49 is positioned on the edge of the ellipsoid (Walkinshaw et al., 1980; Lobel et al., 1985).

Exploration of the interaction of curarimimetic snake toxins with the AcChR has taken two directions. One direction of research is towards the determination of the location of the toxin binding site on the AcChR. Chemical cross-linking of snake toxins to the AcChR indicate that the toxin interacts with the α and the δ subunits of the AcChR (Witzemann et al., 1979; Hucho, 1979; Oswald and Changeux, 1982; Nathanson and Hall, 1980). Electron microscopy and single-particle image averaging show that α-bungarotoxin binds at two regions of the receptor: one (α_1 subunit) adjacent to the δ subunit and the other diametrically across the receptor molecule, ~50 Å away

from the δ subunit on the α_2 subunit (Zingsheim et al., 1982). The distance between bound toxins has been confirmed by us using fluorescence energy transfer techniques (Johnson et al., 1984) and more recently by Kubalek et al. (1987) using image analysis of electron microscope photographs. Finally, a subsequence (residues 173-204) of the AcChR α subunit binds snake curarimimetic toxins, which suggests that this subsequence forms part of the toxin binding site (Wilson and Lentz, 1988).

The second direction of research on the interaction of curarimimetic snake toxins is to define the location of the surface of the toxin that binds to the AcChR. Comparison of the subsequences of curarimimetic snake toxins with noncurarimimetic proteins of similar structure suggests that the residues Trp-25, Arg-33, and Gly-34 (numbered relative to the sequence of siamensis 3 toxin) are essential for neurotoxicity (Low, 1979; Dufton and Hider, 1983). X-ray analyses of the snake toxins reveal conformations of the tip of the central loop (residues 25-35) that resemble the structure of curarimimetic alkaloids (Dufton and Hider, 1983). Synthetic polypeptides that correspond to subsequences of the central loop of the snake toxins bind to the AcChR further suggests that the central loop directly participates in the binding of snake curarimimetic toxins to the AcChR (Juillerat et al., 1982; Ralston et al., 1987; Lentz et al., 1987). Avidin binds to AcChR-bound α-toxins that are biotinylated at Lys 12, Lys 69 and Lys 49, demonstrating that these sites of labeling are not part of the toxin binding surface (Lobel et al., 1985). Solute accessibility to spin labels attached to α-toxin confirm the noninvolvement of Lys 12, Lys 49, and Lys 69 and also show noninvolvement of Lys 35 in the binding surface of α-toxin (Bystrov et al., 1983), when the effects of binding-dependent changes in rotational diffusion

on the solute accessibility are considered (Johnson and Yguerabide, 1985).

In this manuscript, the interaction of curarimimetic snake toxins with the AcChR was defined further. We examined the solute accessibility, the relative proximity to AcChR tryptophans, and the relative proximity to the surface of the lipid membrane of FITC attached to the ϵ-amino groups of four AcChR-bound-α-toxin residues, Lys 23, Lys 35, Lys 49 and Lys 69. We observed equal accessibility of iodide ion to each site of labeling both when the derivatives were free in solution and bound to the receptor. The changes in observed solute quenching could be explained by the changes in rotational diffusion associated with FITC conjugation to the α-toxin and the conjugate binding to the AcChR-enriched membrane fragments (Johnson and Yguerabide, 1985). Consequently, our results indicate that Lys 23, Lys 35, Lys 49 and Lys 69 are not part of the binding surface of the α-toxin.

Measurements of energy transfer between AcChR tryptophans and the sites of labeling of bound-toxin derivatives indicated that Lys 49 is closer to AcChR tryptophans than Lys 23, Lys 35, and Lys 69. The distance between the AcChR tryptophans and the FITC moieties could not be calculated, because the number, the quantum yield, and the A_D of the donor tryptophans are unknown. However, a minimum number of tryptophans that transfer energy can be estimated by assuming that each donor tryptophan transfers all its energy (E = 1) to the FITC moieties and that the extinction coefficients of the tryptophans and FITC at 280 nm are 5,000 and 30,000 $M^{-1}cm^{-1}$, respectively. From Equation 11, at least 12 tryptophans transfer energy to the FITC attached to Lys 49 and 6-7 transfer energy to FITC attached to Lys 23, Lys 35, and Lys 49. Since we observed significantly more energy transfer from the AcChR to the Lys 49 derivative, Lys 49 on the AcChR-bound toxin is closer

to the surface of the receptor than Lys 23, Lys 35, or Lys 69. Similarly, since the magnitude of energy transfer between the AcChR and the AcChR-bound Lys 23, Lys 35 and Lys 69 derivatives was about the same, Lys 23, Lys 35, or Lys 69 of the AcChR-bound α-toxin are about equidistant to the receptor.

Measurements of energy transfer between the surface of the lipid membrane and the sites of labeling on receptor-bound derivatives indicate that the magnitude of the distances of closest approach between the lipid-membrane surface and sites of labeling are in the order Lys 23 (40Å) ≃ Lys 49 (41Å) > Lys 35 (45Å) ≃ Lys 69 (46Å). The equation used to calculate the distances (Equation 12) assumes that the distance, L, is greater than $1.68R_o$ and that the acceptor-lipid probe is randomly distributed on the surface of the lipid membrane (Shaklai et al, 1977). In the present case, the R_os (42-46 Å) were about equal to the Ls (40-46 Å), and acceptor-lipid probes were probably excluded from the volume occupied by the transmembrane domain of the AcChR. The consequence of $L \simeq R_o$ is a reduction of numeric precision, and the consequence of an excluded space on the membrane surface would be to decrease the energy transfer and reduce the calculated distance, L. Thus, assumptions were obviously unsatisfied and, consequently, the calculated distances are imprecise. In spite of the imprecision of our distance estimates, we can minimally use these estimates to define the relative distances of closest approach to the lipid-membrane surface.

Fig. 18 depicts the approximate orientation α-toxin on the receptor, which can be deduced from our solute accessibility and energy transfer studies and the previous observations that the two α-toxins sit on the apical extracellular surface of the AcChR about 50 Å apart with the tip of the central loop of the α-toxin in contact with the receptor. The representation

in Fig. 18 shows the α-toxins with the tip of the major axis in contact with the receptor tilted from a perpendicular membrane projection. The concave surface containing Lys 23 projects away from the central ion channel of the receptor. Because α-toxin tilts, FITC-Lys-23 moiety projects towards the lipid-membrane surface, the FITC-Lys-49 moiety projects tangent to the perimeter of the cylindrical AcChR, and the Lys 49 is about the same distance to the lipid membrane surface as Lys 23. Moreover, because Lys 4 is closer to the tip of the central loop of the α-toxin, Lys 49 is closer to the receptor surface than Lys 23, Lys 35 or Lys 69, which are about equidistance from the receptor. Lys 35 and Lys 69, on the convex surface, project towards the central ion channel of the receptor. Lys 23, Lys 35, Lys 49, and Lys 69 are all completely accessible the bulk solute.

Combined with the previous observations that snake toxins sit on the apical extracellular surface of the AcChR (Zingsheim et al. (1982); Kubalek, et al., 1987), our energy transfer measurements between the surface of the lipid membrane and the AcChR-bound toxins suggest that extracellular protrusion of the AcChR is <40 Å. While some assumptions were not satisfied in our transverse distance calculations, satisfaction of these assumptions would lead to a smaller estimate of the AcChR extracellular protrusion. Other considerations argue against the estimates of the site of AcChR extracellular protrusion provided by image analysis of ordered arrays of AcChR's, which report the extracellular domain to be a cylinder 55-70 Å high and 80-85 Å in diameter (Kistler et al., 1982; Brisson and Unwin, 1985). The calculated volume of such a cylinder would be $3.1\text{-}3.5 \times 10^5$ Å^3 minus $0.12\text{-}0.15 \times 10^3$ Å for the inverted circular-cone-shaped channel (12.5 upper and 3 Å lower radii). The calculated volume from the image analysis studies is

considerably larger than the volume calculated from most proposed amino acid compositions of the extracellular domain ($2.0x10^5$ Å^3) (reviewed by Changeux et al., 1987). (Calculation based on the following assumptions: (1) the first 210 residues of each of the 5 subunits form the extracellular domain, (2) the average residue molecular mass is 115, and (3) the partial specific volume of a hydrated protein is 1.03cm^3/g.) A similar discrepancy occurs upon comparing the calculated volumes from the proposed dimensions of the whole AcChR (Kistler et al., 1982; Brisson and Unwin, 1985) and the known total molecular mass. The published dimensions (cylinder with a 80-85Å diameter and 110-140 Å height) yield a total volume of $6.2\text{-}7.0x10^5$ Å^3 and the published molecular mass (Noda et al., 1982; Claudio et al, 1983; Noda et al., 1983) (M_r=268,078) yields $4.6x10^5$ Å^3. The recent observations that residues 173-204 of the AcChR α subunit form part of the toxin binding site (Wilson and Lentz, 1988) also suggest that the distance between the lipid membrane surface and the toxin binding site is <40 Å. If, as is generally thought (Changeux et al., 1987), one of the transmembrane domains starts at residue 211 and the segment between 204 and 211 projects away from the membrane surface in an extended conformation, the distance between residue 204 and 211 would be 24 Å. Further work defining the overall dimensions of the receptor is clearly required.

Section III

INTRODUCTION

The nicotinic acetylcholine receptor (AcChR) functions as a neurotransmitter-activated cationic channel (see Changeux et al., 1984 for review). The receptor is composed of four different subunits (α, β, τ, δ) which are present with a stoichiometry of α_2, β, τ, δ. All four subunits span the membrane, possess considerable amino acid sequence homology (Noda et al., 1983) and presumably have similar patterns for peptide chain folding and spanning the membrane. Features of the general quaternary structure of the AcChR have been examined by electron microscopy of AcChR enriched membranes obtained from the electric ray, Torpedo (Brisson and Unwin, 1985; Giersig et al., 1986; Unwin et al., 1988). These studies reveal that the five subunits are arranged with pseudo-pentagonal symmetry around a central cavity which is presumed to be the synaptic portion of the ion channel. However, current resolution of the receptor structure by this method is insufficient to distinguish binding sites for small ligands, individual peptide chains and the dimensions of the ion channel within the membrane bilayer.

To understand the molecular mechanism of action of the AcChR, it is necessary to define its structure and delineate the locations of ligand binding sites that modulates its activity. Previous studies have shown that the binding of agonists to two sites, one on each α subunit, opens the channel whereas the competitive binding of antagonists and the snake venom α-toxins, which are peptides of approximately 7000 MW, have been extensively used as markers to localize the agonist/antagonist sites. Electron

microscopy of α-toxin-complexed receptor has shown that the toxins bind each a-subunit on the synaptic surface (Zingsheim et al., 1982; Kubalek et al., 1987). Another approach to ascertaining the location of the agonist/antagonist sites has been to measure intersite distances by fluorescence energy transfer experiments. The results obtained from measuring the distances between fluorescently-labeled toxins (Johnson et al., 1984) and between a fluorescent toxin and a small, reversible antagonist (Johnson et al., 1987) suggested that the agonist/antagonist sites reside near the outer periphery of the receptor molecule rather than close to a central pseud-axis of symmetry perpendicular to the membrane surface.

Another important class of ligands which regulate receptor function are noncompetitive inhibitors (NCI) which are potent blockers of the AcChR both in vivo and in vitro. Several members of this heterogeneous group of compounds, which include the tertiary and quaternary amine local anesthetics, histrionicotoxin and phencyclidine, interact at a site other than the agonist/antagonist sites. A number of electrophysiological studies have led to the "open-channel blockade hypothesis" which postulates that these compounds bind to a specific site(s) within the open ion channel (Neher and Steinbach, 1978; Adams, 1977; Koblin and Lester, 1979). These ligands bind to a high affinity single site per receptor monomer that is allosterically coupled to the agonist/antagonist sites (Heidmann et al., 1983). NCO affinity labeling studies (Kaldany and Karlin, 1983; Muhn and Hucho, 1984; Giradaut et al., 1986, 1987) and the kinetics of NCI binding Oswald et al., 1983) support the hypothesis that NCI ligands bind to a site within the ion channel and that their binding site is contributed by portions of all five subunits. If this model is correct, certain noncompetitive

inhibitors may serve as valuable tools to define the structure of the ion channel component of the AcChR.

In this study, the distances between the high affinity NCI site and the agonist/antagonist sites were measured by fluorescence energy transfer. Energy transfer efficiency was measured between two different donor-acceptor pairs: (1) a fluorescent agonist, Dansyl-C_6-choline and a fluorescent NCI, ethidium and (2) a fluorescent antagonist, BCNI, and ethidium (Fig. 19). In previous studies, we found that ethidium binds with a stoichiometry of one molecule per receptor oligomer and is displaced completely from its binding site by well-characterized NCI ligands such as phencyclidine and histrionicotoxin (Herz et al., 1987). In addition, ethidium binding is allosterically enhanced by the association of agonists and certain antagonists at their primary sites. In the present study, measurement of steady-state fluorescence and fluorescence lifetimes revealed energy transfer. The calculated distances obtained for each donor-acceptor pair using the steady state and lifetime methods are in good agreement.

EXPERIMENTAL PROCEDURES

Materials [^{3}H]Phencyclidine (49.9) Ci/mmol) and ^{125}I-α-bungarotoxin were purchased from New England Nuclear. Ethidium was purchased from Calbiochem-Behring Corp., carbamylcholine and diisopropylfluorophosphate were from Sigma Chemical Co., BCNI was synthesized and characterized as previously described (Bolger et al., 1984). Dansyl-C_6-choline was obtained from the National Institute of Mental Health and PCP was obtained from the National Institute for Drug Abuse. All other reagents were of the highest purity available.

Acetylcholine Receptor Purification. See Section I.

Binding of [^{3}H]PCP. Equilibrium binding of radiolabeled PCP and competition between ethidium and other ligands was measured using the ultracentrifugation procedure described previously (Herz et al., 1987).

Fluorescence Titrations. Steady state fluorescence measurements were made on a Spex Fluorolog 211 interfaced to a Spex DM1B computer. The light source was a 150W xenon-arc lamp and fluorescence was detected by photon counting. Excitation spectra were corrected for wavelength-dependent effects. Typical excitation and emission sites produced a bandpass of 4.6 nm. Titrations were performed in 100 mM NaCl, 10 mM $NaPO_4$, pH 7.4 in 1 cm^2 cuvettes at room temperature. The total dilution from added titrant did not exceed 1% of the total sample volume. To minimize stray light for the determination of ethidium florescence, excitation at 290 nm required the use of a Corning 7-54 filter on the excitation side and a Corning 3-70 cutoff filter on the emission side. In competitive back titrations with PCP, corrections for inner filter effects were not necessary since the total concentration of the energy acceptor, ethidium, was unchanged throughout the experiment. This approach is valid if the bound and free ligand has nearly the same extinction coefficient.

Analysis of Ligand Binding. Ligand association and competition binding experiments were analyzed by a non-linear regression computer program, GRAPH-PAD for a single class of binding sites (Motulsky, 1983).

Fluorescence Lifetime Analysis. Fluorescence lifetimes were determined by the time-correlated single-photon counting technique using a EEY Scientific nanosecond fluorescence spectrofluorometer (La Jolla, CA) equipped with a high-pressure hydrogen arc lamp. Lamp pulse rates were 20 KHz and the timing calibration was 0.42 ns per channel. UV excitation was selected in

order to enhance the contribution of specifically bound Dansyl-C_6-choline. The excitation band was selected with a Corning 7-54 interference filter placed between the sample cuvette and lamp. The emission band of Dansyl-C_6-choline was selected with an Oriel 540 nm narrow band interference filter (no. 5436). The filters used for measurement of the Dansyl-C_6-choline lifetime were selected to minimize interference from ethidium emission. In addition to the chromatic filters, a Polaroid HNP'B dichroic film polarizer (Norwood, MA) was placed in the emission path. The emission polarizer was rotated at an angle of 54^o relative to vertical in order to eliminate anisotropic contributions to the observed decay. Fluorescence decay rats were resolved and assessed as either single or double exponential functions by using the method of moments. The best computer fits were selected on the basis of minimization of χ^2/N values. The effects of light scatter were controlled by subtracting the apparent decay curves of samples that contained all the components of the experimental samples except the fluorophore. The instrumental arrangement and principles of data treatment have been discussed in detail elsewhere (Yguerabide and Yguerabide, 1984; Herz et al., 1987).

Energy Transfer. The efficiency of dipolar resonance energy transfer between a discrete donor and acceptor pair is related to the distance (R) separating the pair by Equation 15 (Forster, 1965).

$$R = R_o(1/E - 1)^{1/6} \qquad (15)$$

where R_o represents the distance at which transfer efficiency equals 50%. R_o (in Å) is calculated from

$$R_o = 9.765 \times 10^3 (\kappa^2 J Q_D n^{-4})^{1/6} \qquad (16)$$

where Q_D denotes the donor quantum yield in the absence of acceptor and n represents the refractive index of the medium between donor and acceptor.

κ^2, the "orientation factor", accounts for the relative orientation in space of the donor emission and acceptor absorption transition dipoles. The overlap integral, J, represents the degree of resonance overlap between excited state donor and acceptor dipoles and is evaluated as the integrated area of overlap between the donor emission spectrum, $I_D(\lambda)$ and is given by

$$J = \frac{\int I_D(\lambda)\, e_A(\lambda)\, \lambda^4\, d\lambda}{\int I_D(\lambda)\, d\lambda} \qquad (17)$$

where λ is the wavelength in units of cm.

In the typical case where donor and acceptor are at separate sites on a macromolecule, the efficiency of energy transfer (E) can be measured as the extent of the reduction of the donor quantum yield or fluorescence lifetime:

$$E = 1 - \frac{I_{DA}}{I_D} \qquad 1 - \frac{\tau_{DA}}{\tau_D} \qquad (18)$$

where I_{DA} and I_D are the fluorescence intensities of the donor (D) in the presence and absence of the acceptor (A), and τ_{DA} and τ_D are the fluorescence lifetimes of the donor in the presence and absence of acceptor, respectively.

When multiple lifetimes are observed, the transfer efficiency can be calculated from:

$$E = 1 - \frac{\Sigma a_i\, \tau_i}{\Sigma a_i^{o}\, \tau_i} \qquad (19)$$

The terms in the numerator and denominator represent the total fluorescence intensity in the presence and absence of acceptor, respectively. The efficiency of transfer is calculated from the experimental amplitudes (a_i)

and lifetimes (τ_i) of each component.

Analysis of the limiting emission anisotropies of the donor and acceptor can provide upper and lower limiting values for κ^2 (Dale et al., 1979). When both axial depolarization factors are positive, the following equations apply:

$$\kappa^2_{MAX} = 2/3(1+\langle d_D^X\rangle+\langle d_A^X\rangle+3\langle d_D^X\rangle\langle d_A^X\rangle) \qquad (20)$$

$$\kappa^2_{MIN} = 2/3[1-(\langle d_D^X\rangle+\langle d_A^X\rangle)/2] \qquad (21)$$

where $\langle d_D^X\rangle$ and $\langle d_A^X\rangle$ cenote the axial depolarization factors of the donor and acceptor, respectively. These depolarization factors were estimated from the individual limiting emission anisotropies of BCNI, Dansyl-C_6-choline (free in solution) and ethidium (bound) by the following equation:

$$\frac{r_o}{0.4} = \langle d^X\rangle^2 \qquad (22)$$

where r_o is the individual limiting emission anisotropy. The limiting anisotropies were obtained by measurement of the steady-state emission anisotropy as a function of viscosity and subsequent extrapolation of a Perrin plot to infinite viscosity (data not shown).

The maximum and minimum values of κ^2 were used to calculate the extreme range of R_o'S:

$$R_{o(MIN)} = \frac{[\kappa^2_{MIN}]^{1/6}\ R_o(2/3)}{2/3} \qquad (23)$$

$$R_{o(MAX)} = \frac{[\kappa^2_{MAX}]^{1/6}\ R_o(2/3)}{2/3} \qquad (24)$$

where $R_o(2/3)$ is the estimated R_o calculated using $\kappa^2 = 2/3$ in Equation 21. The corrected transfer efficiency, E_c, and extreme R_o'S from the above were used to calculate a range of distances between the sites:

$$R_{(MIN)} = [(1/E_c)-1]^{1/6} R_{o(MIN)} \quad (25)$$

$$R_{(MAX)} = [(1/E_c)-1]^{1/6} R_{o(MAX)} \quad (26)$$

In the case where 2 donors transfer energy to one acceptor and equal quenching of both donors occurs, then Equation 20 may be used to relate transfer efficiency to intersite distances (Cantley and Hammes, 1976).

RESULTS

Spectroscopic Characterization of Donor and Acceptor Pairs. The absorption spectrum of ethidium bound to the AcChR overlaps the fluorescence emission spectra of both Dansyl-C_6-choline and BCNI bound to the agonist/antagonist sites. The spectral relationships for each of these donor-acceptor pairs are shown in Fig. 20. To eliminate contributions from light scatter, the fluorescence emission spectra for Dansyl-C_6-choline and BCNI are difference spectra obtained by subtracting the spectra obtained in the presence of 5-10 fold excess α-toxin from samples containing receptor, PCP and either the fluorescent agonist or antagonist. The fluorescence emission maximum of Dansyl-C_6-choline appears at 532 nm, a shift of 25 nm from the 557 nm maxima observed in buffer. Bound BCNI exhibits an emission spectrum similar to Dansyl-C_6-choline, demonstrating a maxima at 533 nm. For each pair, the fluorescence emission envelope of the donor around the maximum is substantially free of acceptor fluorescence contamination, thus permitting donor quenching to reflect energy transfer. However, the emission maximum of ethidium is influenced by the long wavelength tail of donor fluorescence, making quantitation of acceptor sensitization more difficult.

The major absorbance maximum of BCNI when bound to AcChR is found by difference spectroscopy at 485 nm. A minor absorbance band centered at 348 nm is also observed. These values are similar to those values observed in the excitation spectra of BCNI in buffer. In calculating the overlap integrals for the two donor-acceptor pairs, the spectral properties of ethidium bound to the NCI site were employed.

The published quantum yield of bound BCNI is 0.075 (Bolger et al., 1984). The spectroscopic constants utilized to calculate the Forster critical transfer distance (R_o) from Equation 16 are shown in Table VII. The spectral overlap integral (J), quantum yields in the absence of acceptor (Q_D), and the orientation factor (κ^2), yield similar R_o (2/3) values for the Dansyl-C_6-choline/ethidium (29.1Å) and BCNI/ethidium (26.2Å) donor-acceptor pairs (Table IX). Thus, assuming a minimum detection level of 5% for energy transfer efficiency, these donor-acceptor pairs can be utilized to measure intersite distances up to 53Å.

Allosteric Interactions between Fluorescent Ligands Bound to the Agonist and Noncompetitive Inhibitor Sites. One criterion which must be considered in the selection of fluorescent donor-acceptor pairs for the AcChR is the well-documented allosteric interactions between the agonist/antagonist and high affinity NCI sites. We previously demonstrated that binding of agonists enhances ethidium binding by converting the NCI site to a high affinity state (Herz et al., 1987). To determine whether similar allosteric interactions occur with BCNI and Dansyl-C_6-choline, we determined the effect of these ligands on ethidium occupation of the NCI site. Binding of ethidium was directly monitored by measuring changes in its fluorescence signal at 590 nm upon excitation at 290 nm. Excitation at 290 nm also resulted in

excitation of BCNI or Dansyl-C_6-choline since spectral overlap occurs between AcChR tryptophanyl emission and fluorescent antagonist and agonist absorption, thus allowing dipolar fluorescence energy transfer to occur. nevertheless, the fractional contribution of the BCNI and Dansyl-C_6-choline fluorescence emission in the region of maximal ethidium emission (590 nm) was small and did not preclude measurement of the signal of interest. Specific fluorescence due to changes in ethidium occupation were calculated by correcting for nonspecific changes that occurred in the presence of excess PCP, a nonfluorescent ligand which is competitive with ethidium and also enhances agonist binding affinities (Herz et al., 1987).

Titration of the receptor enriched membranes with BCNI resulted in a substantial increase in ethidium fluorescence (Fig. 21A). Computer fitting of the data assuming a single class of binding sites yielded a BCNI dissociation constant of 0.25 μM. This value agrees with values previously determined by direct fluorescence titration (0.22 μM) and by competition with the initial rate of α-toxin binding (0.25 μM) (Bolger et al., 1984).

The fluorescence of ethidium also increased due to association of Dansyl-C_6-choline with the agonist sites. In contrast to the hyperbolic curve observed with BCNI, a linear increase in fluorescence intensity occurred until the saturation level was reached. The difference in the titration profiles can be ascribed to the concentration of ligand binding sites being greater than the dissociation constant for Dansyl-C_6-choline binding. Thus, both BCNI and Dansyl-C_6-choline act as positive allosteric modulators of the NCI site by increasing the affinity of ethidium binding. Similar experiments showed that the association of either BCNI or Dansyl-C_6-choline with AcChR also increased the affinity of the NCI site for ^{3}H-PCP

(data not shown).

Energy Transfer between BCNI and Ethidium. Energy transfer was measured by steady-state titrations in which BCNI was employed as an energy donor bound to the agonist sites and ethidium was used as the energy acceptor bound to the NCI site. To ensure that changes in donor quantum yield were due to energy transfer and not differences in ligand occupation, a competitive displacement method was used. The fluorescence of the donor was initially measured in the presence of the acceptor bound to the AcChR after equilibration with both fluorescent ligands. Then, increasing amounts of a NCI ligand without overlapping absorption and fluorescent spectra (PCP) were added to the cuvette and the fluorescence of the solution was monitored after equilibration. As will be discussed later, this back titration approach minimized changes in donor occupation at the agonist-antagonist site.

As seen in Fig. 22A, addition of PCP decreased the intensity of ethidium emission (λ = 540-650 nm) and concomitantly increased BCNI fluorescence (450-540 nm). An isosbestic point at 540- nm was observed. These results show that displacement of the energy acceptor from the NCI sites increased donor fluorescence. In Fig. 22B, a parallel titration was carried out in which carbamylcholine was instituted as a nonabsorbing analog for BCNI. The emission spectra show a progressive reduction in intensity and red spectral shift as a function of increasing PCP concentrations. These changes solely reflect displacement of ethidium from the NCI site by PCP and are also evident in the spectra in Fig. 22A. Most importantly, no changes in intensity are observed in the spectral region of donor emission (λ_{MAX} = 532 nm). Another control is provided by addition of PCP to AcChR membranes in the presence of BCNI or ethidium emission intensities as a result of PCP

addition. This result is expected since neither BCNI nor ethidium is specifically bound to their respective sits under these conditions, and further confirms that the increase in BCNI fluorescence emission is due to the specific displacement of ethidium from the NCI site. The changes occurring in the 450-550 spectral region were more clearly resolved by creating difference spectra (Fig. 22D) that eliminated the contribution of ethidium fluorescence. Each spectra in Fig. 22B at a given PCP concentration was subtracted from its counterpart in Fig. 22A. The resulting series of spectra have a shape and emission maximum (λ_{MAX} = 525 nm) characteristic of BCNI bound to AcChR agonist sites. The specific change in donor fluorescence at each PCP concentration was calculated by subtracting the intensity at 525 nm defined in Fig. 22C. The concentration dependence of the increase in BCNI florescence exhibits a hyperbolic shape and is saturable (Fig. 23). The apparent K_I for PCP is estimated to be between 1.0 and 2.0 μM which is in good agreement with the K_I observed for PCP inhibition of ethidium binding to NCI site in the presence of other agonists (Herz et al., 1987).

Transfer efficiencies for each concentration of PCP were calculated using the fluorescence determined in the presence of 50 μM PCP as representing the unquenched signal. The maximum donor quenching efficiency was found to be 27 ±3%. The transfer efficiency measured by steady-state techniques must be corrected for acceptor labeling stoichiometry when the stoichiometry is less than one-to-one (Fairclough and Cantor, 1978). If the fraction of AcChR's occupied with an acceptor is f_a, then the corrected transfer efficiency, E_c, that would be observed when all AcChR's had an acceptor bound is given by:

$$E_c = E_{obs}/f_a \qquad (27)$$

To obtain E_o, the data from Fig. 23A were plotted as the observed transfer efficiency as a function of acceptor occupancy. The fraction of ethidium bound at each concentration of PCP was determined according to the following equation:

$$\frac{[RL]}{B_{MAX}} = \frac{L/K_E}{(1 + L/K_E + I/K_I)} \qquad (28)$$

where L is the concentration of ethidium (1.0 μM), I is the concentration of PCP, K_E is the dissociation constant for ethidium in the desensitized state (0.25 μM), K_I is the dissociation constant for PCP in the presence of agonist (0.4 μM), [RL] is the concentration of receptor-ethidium complexes and B_{MAX} is the total concentration of receptor NCI sites. As seen in Fig. 23B, the observed transfer efficiency increased in direct proportion to the calculated acceptor occupancy. Linear extrapolation of acceptor occupancy to 100% yielded a corrected transfer efficiency of 38 ±5%.

Nanosecond Lifetimes Measurements of Donor. The fluorescence decay rate for Dansyl-C_6-choline in buffer obeys a single exponential behavior with a lifetime of 3.2 ns (Fig. 24A). In contrast, Dansyl-C_6-choline bound to the agonist sites in the presence of a nonfluorescent noncompetitive inhibitor (PCP) exhibits significantly longer lifetimes and is best described by double-exponential decay process (Fig. 24B). The fluorescence decay is characterized by two lifetimes (τ_1 = 6.7, τ_2 = 17.1 ns) in which the shorter lifetime component contributes the greater amplitude (a_1/a_2 = 2.4). The longer lifetimes observed for bound Dansyl-C_6-choline are consistent with the

blue shifted emission maxima observed in steady-state spectra and reflect a more hydrophobic environment of the DANSYL fluorophore upon binding the receptor. Lifetimes originating from nonspecific interactions of Dansyl-C_6-choline with AcChR membranes were evaluated by addition of either a stoichiometric excess of α-toxin or a large excess of carbamylcholine. Nearly identical double-exponential decay rates were obtained in the presence of both competitive inhibitors of Dansyl-C_6-choline (Fig. 24C,D). The dominant component (a_1/a_2 = 7.8) of these rates had a short lifetime (3.4-3.6 ns) characteristic of Dansyl-C_6-choline in buffer. This indicated that Dansyl-C_6-choline displaced from its binding site by competitive inhibitors primarily transferred into the aqueous phase. In the presence of ethidium, Dansyl-C_6-choline bound to the agonist sites showed a significant reduction in both lifetime values. Analysis of the fluorescence decay data by computer-fitting revealed a double-exponential rate process (τ_1 = 5.6, τ_2 = 14.4 ns). The relative contributions of the short and long lifetime components remained comparable in the presence of the energy acceptor (a_1,a_2 = 3.8). The specificity of the change due to ethidium binding was tested for reversibility by addition of excess nonfluorescent noncompetitive inhibitor. In the presence of 200 uM PCP, both short and long lifetime components were restored to values nearly identical (97% of original) to those observed in the absence of the energy acceptor (τ_1 = 6.5, τ_2 = 16.7 ns) and retained an identical amplitude ratio (a_1/a_2 = 2.5).

Thus, the reductions in both the short and long lifetimes reflect energy transfer from Dansyl-C_6-choline bound to the agonist sites to ethidium at the NCI site. The transfer efficiency was calculated from Equation 19 accounting for the multiple exponential amplitudes and lifetimes described above. The

efficiency of transfer was found to be 24.0%. Steady-state spectra of these samples obtained prior to lifetime measurements provided complementary data demonstrating donor quenching in the presence of ethidium. The calculated transfer efficiency of ethidium from the ratio of Dansyl-C_6-choline intensifies (530 nm) in the presence of ethidium vs. PCP bound to the NCi site was also 24%. Thus, the values obtained by nanosecond lifetime measurements are in agreement with those obtained by steady state methods. Linear extrapolation to 100% acceptor occupancy yielded a transfer efficiency of 33.8%.

The short fluorescence lifetime of the BCNI donor (τ = 1 ns) when bound to the AcChR in the absence or presence of ethidium is close to the duration of the lamp pulse, precluding an accurate measure of lifetime changes associated with the addition of a noncompetitive inhibitor.

Range of Distances between Agonist and NCI Sites. Analysis of the limiting emission anisotropies of both the donor and acceptor can be utilized to place constraints on the value of the orientation factor, κ^2. Measurements of steady-state polarized fluorescence for Dansyl-C_6-choline, BCNI, and ethidium yielded limiting anisotropies (A_o) of 0.30, 0.23 and 0.32, respectively. The axial depolarization factors calculated from these anisotropies using equation 8 were 0.87, 0.75 and 0.89. These factors were in turn used to calculate maximum and minimum values for κ^2 using equations 6 and 7. For the Dansyl-C_6-choline-ethidium pair, the orientation factor has values of $0.07 < \kappa^2 < 2.39$ while the BCNI-ethidium pair has a range of $0.12 < \kappa^2 < 2.20$ (Table IX).

The corrected transfer efficiency, E_c, and the range of R_o's (Dale et al., 1979) obtained from Equations 23 and 24 were used to calculate a range

of distances between the donor and acceptor sites (Equations 25 and 26) assuming equivalent quenching of each donor (Table IX). In the case of the BCNI-ethidium pair, for which a 38% corrected transfer efficiency is observed based on steady-state donor quenching, we calculate intersite distances of 21 $\leq R \leq$35Å. For the DNS-C_6-choline-ethidium pair, (E_c = 34%), we calculate distances over a range of 22 < R < 40Å based upon steady-state data. The calculation of transfer efficiencies from the Dansyl-C_6-choline lifetime data depends upon the origin of the short and long components of the double-exponential decay. If the fluorescence properties of DNS-C_6-choline bound to each of two α-subunits are identical, and both the α_1 and α_2 subunit sites gives rise to a double-exponential decay (Model I), then the transfer efficiency may be calculated using Equation 19. The transfer efficiency calculated by this method (E = 0.24) and the intersite distances obtained (R(2/3) = 32Å) are identical to that obtained by steady-state methods (Table IX). In contrast, it is possible that *differences* between the α_1 and α_2 subsites give rise distinct lifetimes associated with each site. In this case, we can arbitrarily assign the short component to α_1 and the long component to α_2 (Model II). This model further assumes that the quantum yields associated with DNS-C_6-choline at each individual α-subunit will be proportional to lifetime since this relationship has been defined for a DANSYL model fluorophore (Li et al., 1975). The transfer efficiencies for Model II calculated by Equation 18 were found to be significantly less than those obtained in Model I ($E_{\alpha 1}$ = 0.18, $E_{\alpha 2}$ = 0.15) (Table VII. The intersite distance calculated for Dansyl-C_6-choline/Ethidium at the α_1 subunit did not differ from Model I (R(2/3) = 32Å), while a slightly greater intersite distance of 38Å (R(2/3)) was found for the α_2-subunit (Table IX). The

ranges of distances generated by the Dale-Eisinger analysis are conservative estimates and it is likely that the actual distance is a result of energy transfer where fluorophore motion is less restricted ($\kappa_2 = 2/3$) (Fairclough and Cantor, 1978). Under these conditions, R = 33Å for Dansyl-C_6-choline and R = 26Å for BCNI.

Table VII

Energy Transfer Parameters for Donor-Ethidium Pairs on the Acetylcholine Receptor

Donor	Q^a_D	J^b (cm^6/mol)	E^c_{obs}	E^d_c
DNS-C_6-choline				
Model I[e]	0.14	2.87 x 10^{-14}	0.24	0.34
Model II[f]				
α_1	0.08	2.87 x 10^{-14}	0.18	0.25
α_2	0.20	2.87 x 10^{-14}	0.15	0.21
BCNI	0.075	3.08 x 10^{-14}	0.27	0.38

[a]Quantum yields were determined using quinine sulfate in 0.1 N H_2SO_4 as a reference (Q = 0.7).

[b]Calculated employing excitation spectra of ethidium bound to AcChR and assuming an extinction coefficient (E_{520}) of 6,600 cm^{-1} M^{-1} and n = 1.6.

[c]Maximum experimentally observed transfer efficiency at sub-maximal occupancy levels.

[d]Corrected efficiency calculated by extrapolation of acceptor occupancy to 100%.

[e]Model I assumes that the fluorescence of DNS-C_6-choline bound to each of the two α-subunits is identical and that each site gives rise to a short (J = 6.7 ns) and long (t = 17.1 ns) lifetime component. Transfer efficiency was calculated from the lifetime data by substitution of the resolved amplitudes (a_1) and lifetimes (t_1) into Eq. 5.

[f]Model II assumes that the short and long lifetimes each are derived from fluorophores bound to non-equivalent α_1 and α_2 subunit sites. The short lifetime (t = 6.7 ns) is arbitrarily assigned as α_2. Transfer efficiencies were calculated independently for α_1 and α_2 using Eq. 4.

Table VIII.

Fluorescence Amplitudes and Lifetimes of Dansyl-C_6-choline in the absence and presence of Ethidium.

LIGANDS[a]	a_1	t_1	a_2	t_2	a_1/a_2
DNS-C_6 in buffer	1.00	3.2	-	-	-
DNS-C_6 + PCP + AcChR	0.70	6.7	0.30	17.1	2.3
DNS-C_6 + α-toxin + PCP + AcChR	0.88	3.4	0.12	17.9	7.3
DNS-C_6 + CARB + Eth + AcChR	0.88	3.6	0.12	18.2	7.3
DNS-C_6 + Eth + AcChR	0.79	5.5	0.21	14.5	3.8
DNS-C_6 + Eth + PCP +AcChR	0.72	6.5	0.28	16.7	2.6

[a]Concentration employed in the above measurements were: AcChR, 1.0 μM α-toxin sites; DNS-C_6, 1.0 μM; PCP, 200 μM; α-toxin, 10.0 μM; carbamylcholine, 1 mM; ethidium, 1.0 μM.

Table IX.

Agonist-NCI Intersite Distances for Donor-Ethidium Pairs on the Acetylcholine Receptor.

LIGANDS	κ^2_{min}	κ^2_{max}	$R_o(2/3)$	$R_o(min)$	$R_o(max)$	R(2/3)
DANSYL-						
Ethidium						
Model I[a]	0.073	2.39	29.1	19.8	36.0	33
Model II[b]						
α_1	0.073	2.39	26.5	18.3	32.8	32
α_2	0.073	2.39	30.9	21.4	38.2	38
BCNI-						
Ethidium	0.120	2.20	26.2	19.7	32.0	26

[a]Model I assumes that the fluorescence of DNS-C_6-choline bound to each of the two α-subunits is identical and that each site gives rise to a short (τ = 6.7 ns) and long (τ = 17.1 ns) lifetime component. Transfer efficiency was calculated from the lifetime data by substitution of the resolved amplitudes (a_1) and lifetimes (t_1) into Eq. 5. Distances were calculated according to Eqtn. 15, 20, and 25 assuming equivalent quenching of donors bound to each α-subunit.

[b]Model II assumes that the short and long lifetimes each originate from distinct α-subunits. The short lifetime (τ = 6.7 ns) is arbitrarily assigned as α_1 and α_2 using Eq. 19 and distances were individually calculated from Eqtn. 15, 25 and 26.

Fig. 19. Structures of the fluorescent reversible ligands employed as probes of the agonist/antagonist and high-affinity NCI sites on the AcChR.

Dansyl-C_6-choline

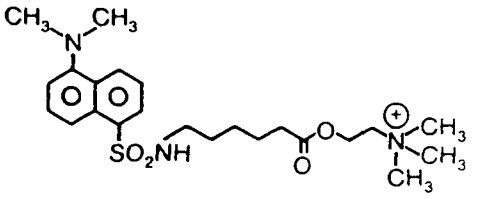

BCNI

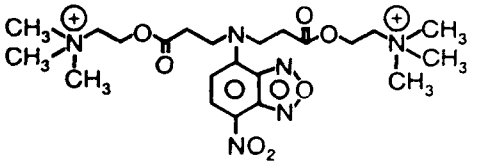

Ethidium

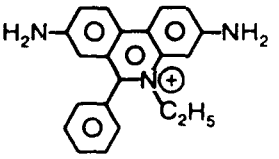

Fig. 20. Spectral relationships characterizing donor-acceptor energy transfer pairs on the acetylcholine receptor. The relationships for the BCNI-ethidium (A), and Dansyl-C_6-choline-ethidium (B) are illustrated. The absorption (solid lines) and emission (dashed lines) spectra for each ligand are shown. The absorption spectra are presented as extinction coefficients (M^{-1}-cm^{-1}) while the emission spectra intensities are in arbitrary units and do not reflect the relative quantum yields of the donor and acceptor. The cross-hatched area indicates the region of overlap between donor and acceptor absorption spectra. The near UV absorption band of ethidium is not shown (300-400 nm).

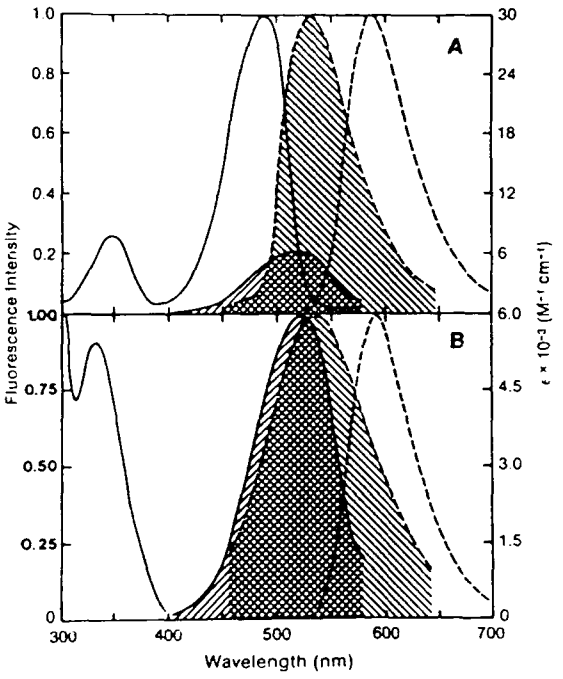

Fig. 21. Allosteric Interactions between Agonist/Antagonist and NCI Fluorescent Ligands. Increase in ethidium fluorescence due to interaction of either (A) BCNI, or (B) Dansyl-C_6-choline, with the agonist/antagonist sites. The excitation and emission wavelengths were 290 nm and 590 nm, respectively. AcChR enriched membranes (0.4 μM α-toxin sites) and ethidium (1.0 μM) were suspended in 100 mM NaCl, 10 mM sodium phosphate at pH 7.4

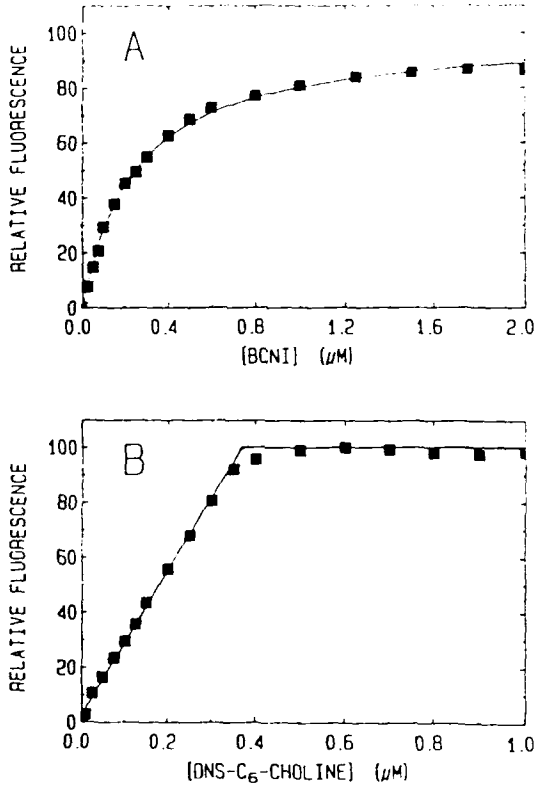

Fig. 22. Energy transfer between BCNI and Ethidium Bound to the AcChR. Fluorescence emission spectra were collected in a range that included donor and acceptor emission. AcChR-enriched membranes (0.4 μM α-toxin sites) were incubated with the following ligands for 1 hr at 25°C prior to back titration with PCP: (A) BCNI (2.0 μM) and ethidium (1.0 μM); B) carbamylcholine (200 μM) and ethidium (1.0 μM), C) BCNI (2.0 μM) α-toxin (4.0 μM), and ethidium (1.0 μM). The excitation wavelength was 290 nm. All titrations were conducted in 100 mM NaCl, 10 mM Na phosphate, pH 7.4. The numbered spectra correspond to PCP concentrations of 1) 0.0 μM; 2) 0.5 μM; 3) 1.0 μM; 4) 2.0 μM; 5) 4.0 μM; 6) 10.0 μM; and 7) 50.0 μM.

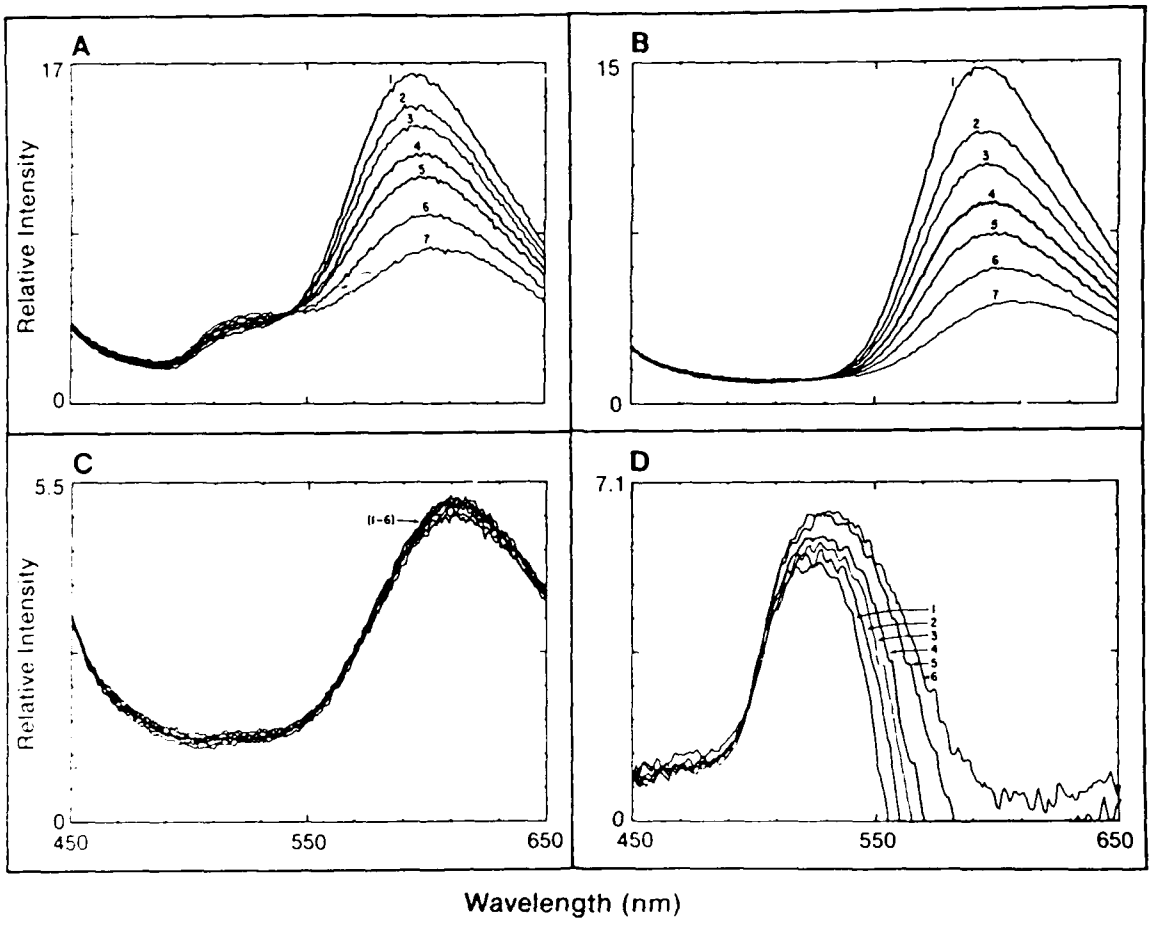

Fig. 23. Transfer efficiencies for BCNI-ethidium pair as a function of acceptor occupancy levels. A) Specific change in fluorescence intensity of BCNI at 525 nm upon titration of AcChR-BCNI-ethidium complexes with PCP. The apparent (K_1 = 1.2 μM for PCP. The fluorescence increase reflects the loss of donor quenching due to displacement of acceptor from NCI site. B) The observed transfer efficiencies plotted as a function of calculated ethidium occupation. Transfer efficiencies were determined for acceptor occupancy levels of 13, 27, 40, 53, 64, 80% of saturation.

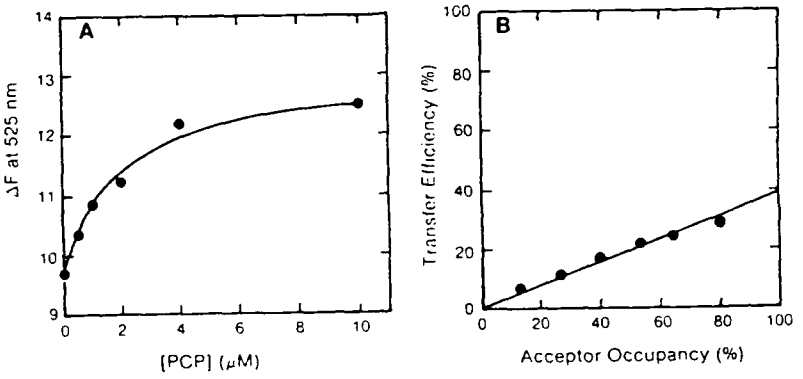

Fig. 24. Nanosecond fluorescence decay rates of Dansyl-C_6-choline specifically bound to the agonist sites on the AcChR. A) Single exponential fluorescence decay of Dansyl-C_6-choline in buffer alone; B) double-exponential fluorescence decay of Dansyl-C_6-choline bound to AcChR membranes (1.0 μM α-toxin sites) in the presence of PCP (200 μM); C) double-exponential fluorescence decay observed for Dansyl-C_6-choline (1.0 μM), AcChR (1.0 μM α-toxin sites) α-toxin (10.0 μM) and PCP (200 μM); D) double-exponential fluorescence decay curve fit to data for Dansyl-C_6-choline (1.0 μM), carbamylcholine (1.0 mM), AcChR (1.0 M α-toxin binding sites) and ethidium (1.0 μM). Each panel (A-D) shows the shape of the lamp pulse (dashed lines), the raw data points, and the computer calculated decay curves (solid lines) obtained by deconvolution of the experimental decay data with the lamp pulse by the method of moments. Deviations of the experimental data from the single or double-exponential decay function are shown in the residual plots above each panel. Values for the fluorescence lifetimes (t) and amplitudes (a_1) are given in Table VIII.

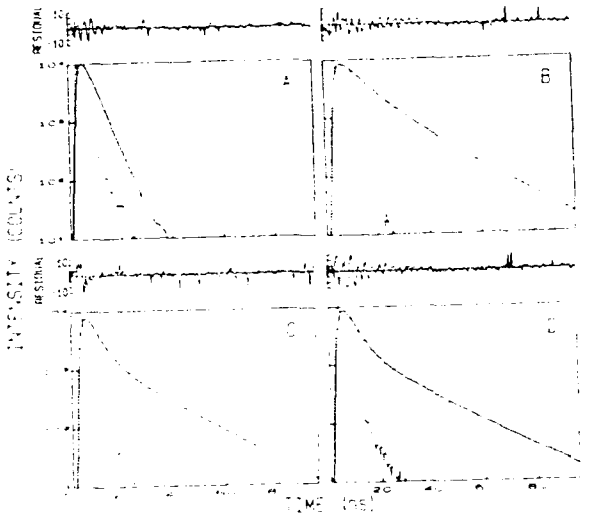

Fig. 25. Reduction in the fluorescence of Dansyl-C_6-choline bound to AcChR agonist sites due to ethidium association at the NCI site. The double-exponential nanosecond decay rates of Dansyl-C_6-choline (1.0 μM) obtained the presence of AcChR-enriched membranes (1.0 μM α-toxin sites), and A) ethidium (1.0 μM) or B) ethidium (1.0 μM) and PCP (200 μM). Samples were equilibrated for 1 hr prior to the data collection interval. Each panel shows lamp pulse (dashed lines), data points, computer fit (solid line) and residual plot as described in Fig. 23.

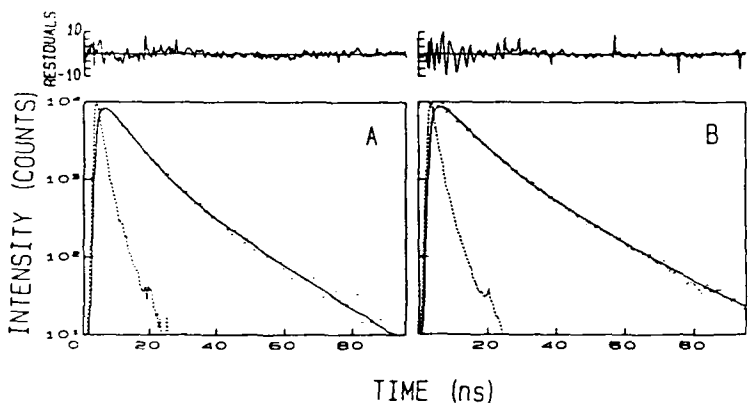

Fig. 26. Dependence of the Transverse Depth of NCI site on Agonist-Agonist Intersite. Distance. The distance relationships between the agonist binding sites and the transverse distance of the NCI site are modelled. The two agonist sites are assumed to be equally distant from the membrane bilayer surface and symmetrically located with respect to the NCI binding site. The three curves define the spatial relationships for the R(2/3), $R_{(MAX)}$ and $R_{(MIN)}$ values determined in this study for the Dansyl-C_6-choline-ethidium pair. The transverse distances for the BCNI-ethidium pair lie within the range defined for Dansyl-C_6-choline-ethidium. The solid line is defined by R(2/3) = 32 Å, the dotted line by $R_{(MIN)}$ = 22 Å, and the dashed line by $R_{(MAX)}$ = 40 Å.

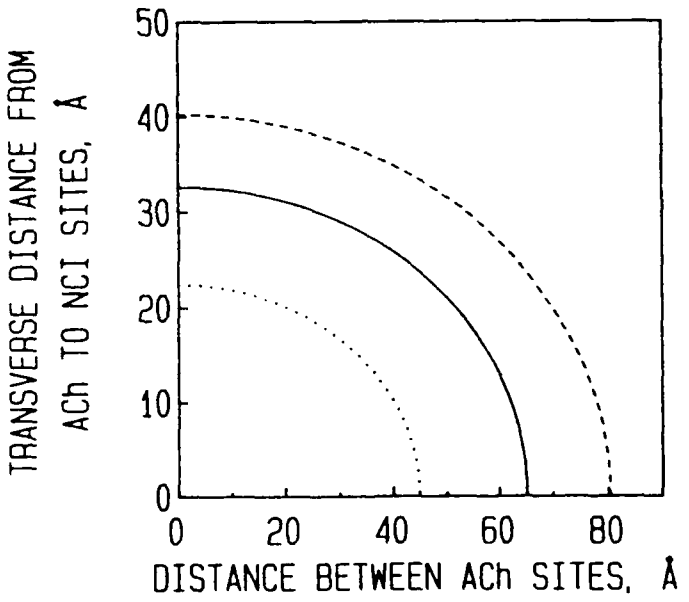

Fig. 27. Model of Acetylcholine Receptor structure showing possible locations for agonist and NCI sites. The molecular dimensions and overall shape of the AcChR are based upon the data of Unwin et al. (1988) and Toyoshima and Unwin (1988). The average agonist-NCI intersite distance of 30 Å determined in this study is drawn to scale. The two agonist sites are positioned symmetrically with respect to the central axis of the AcChR. The inner and outer lateral limits of the agonist boxes define agonist-agonist intersite distances of 30 Å and 50 Å, respectively, while the vertical limits are 20 Å and 26 Å from the synaptic membrane surface. A possible mode of toxin-receptor interaction is shown on the left AcChR in which one α-toxin molecule is bound to each α-subunit. Only the peptide backbone of the toxins are shown. The dimensions of the toxin molecules are drawn to scale with respect to the receptor. However, no absolute orientation of the toxin on the receptor is implied nor are we attempting to define exposed or buried portions of the toxin structure. Unresolved dimensions of the AcChR for which there is no accurate data for denoted by dashed lines.

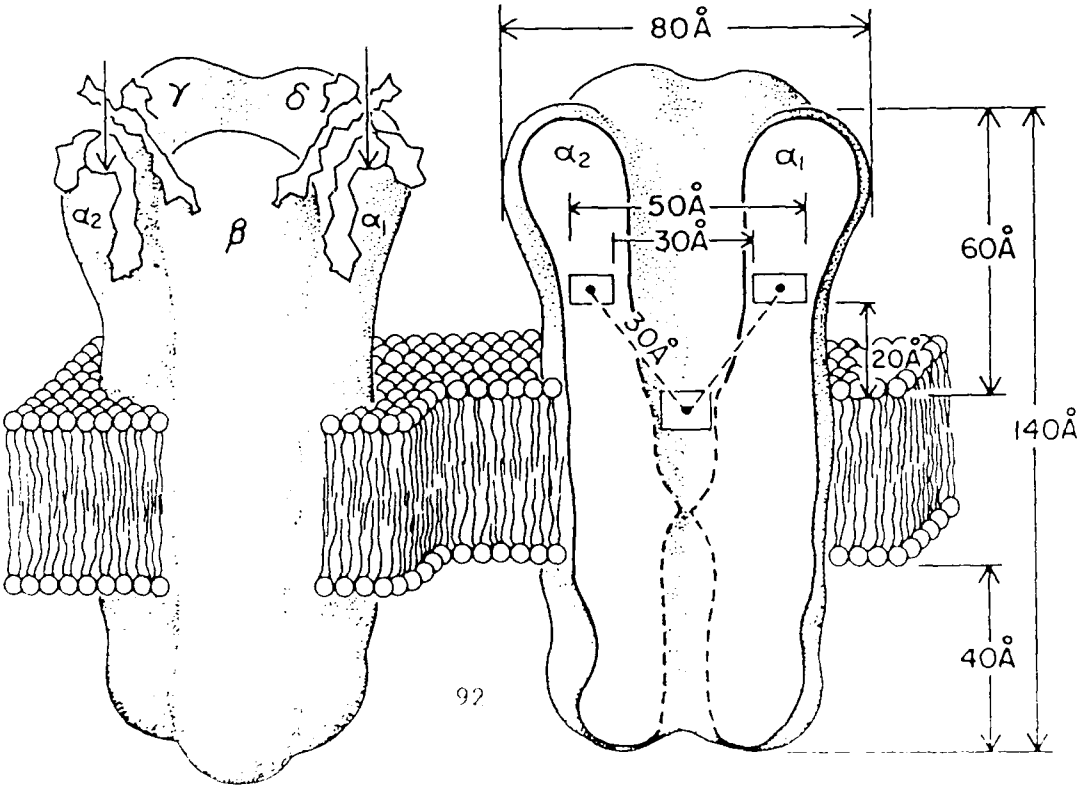

DISCUSSION

In this study, we have utilized fluorescence energy transfer to define the spatial relationships between the agonist/antagonist sites and the allosterically coupled NCI site. We have employed small, reversible ligands that are well-characterized with respect to site specificity, stoichiometry, and affinity (Waksman et al., 1980; Heidmann and Changeux, 1979; Bolger et al., 1984; Herz et al., 1987). energy transfer was measured using two different experimental methodologies for two different combinations of donor-acceptor pairs. Steady-state measurements using the competitive displacement method were employed for both the BCNI-ethidium and Dansyl-C_6-choline-ethidium pairs. In addition, measurements of donor lifetime were made for the Dansyl-C_6-choline-ethidium pair. The results obtained from these independent techniques were in good agreement. We calculated an R(2/3) of 33Å for the Dansyl-C_6-choline-ethidium pair and 26Å for BCNI-ethidium.

Since the agonist and NCI sites on the AcChR are allosterically coupled, it was important in steady-state experiments to insure that titration with the fluorescent acceptor did not alter the occupation levels of the fluorescent donor. In order to insure that changes in donor quantum yield were in fact due to energy transfer, a competitive displacement method was used. PCP, a prototypic nonfluorescent ligand for the NCI site was used as a competitive inhibitor in back titrations to dissociate the fluorescent energy acceptor. Nonspecific changes in donor fluorescence were not detected. Thus, the NCI site remained fully occupied with either ethidium or PCP throughout the titration. Accordingly, the affinity and occupation of the donor site remained constant during the back-titration.

While measurements of donor quenching represent a direct assay for energy

transfer, other factors can also affect observed donor fluorescence. A conformational change in the AcChR caused by binding of the acceptor could produce changes in the environment of the donor binding site and hence alter its fluorescent intensity. This possibility can be minimized since the binding of either PCP or ethidium convert the AcChR to the same desensitized state exhibiting increased agonist affinity (Herz et al., 1987). Thus, changes in conformation as reflected in agonist affinity should not occur when bound ethidium was displaced from the NCI site by a ligand preferring the same receptor state.

The accuracy of the distance estimates obtained in our fluorescence experiments depend upon several factors. Among these, the dipole orientation factor, κ^2, is the most uncertain quantity in the calculation. Through measurements of donor and acceptor limiting anisotropy, we have been able to limit κ^2 values and thereby define the uncertainties in the calculated distances. The uncertainty is diminished below the values suggested by the consideration of limiting anisotropies by the use of two different donor-acceptor pairs at the same sites. It is unlikely that the relative orientation of the emission dipole of each donor is the same when bound to the agonist sites. Since individual intersite distances determined from the two donor-acceptor pairs are in good agreement, this indicates that the effect of the orientation factor on the calculated distance should be small.

When 2 donors and 1 acceptor are present on the same macromolecule, a geometric arrangement of the binding sites can be postulated to relate the measured energy transfer efficiencies to intersite distances (Matsumoto and Hammes, 1975). The efficiency of energy transfer from each agonist site will depend on its position relative to the energy acceptor. In addition, since two

fluorescence lifetimes were observed for Dansyl-C_6-choline donors bound to the agonist sites, at least two interpretations must be considered. The two lifetimes could reflect two microenvironments at each α-subunit site (Model I). In this model, we postulate that the fluorescence of DNS-C_6-choline bound to the α_1 and α_2 subunits of the AcChR is identical and that the fluorescence from each subunit site is composed of a short (τ = 6.7 ns) and long (τ = 17.1 ns) lifetime component. Alternatively, the double-exponential fluorescence decay could reflect two distinct agonist sites. In Model II, the short lifetime is derived entirely from one α-subunit (α_1) and the long lifetime originates from the α_2 subunit. Model III are lifetime bound and on free in solution. Model I is more likely for several reasons. First, previous examples of double-exponential decay rates for DANSYL-ligands bound to a single site have been reported (Berman et al., 1980; Lehrer et al., 1981). In these studies the multiple fluorescence lifetimes were the result of multiple fluorophore conformations because the probes were unambiguously bound to single sites on each protein. In this study, the acyl chain linking the DANSYL moiety to the choline-ester group may allow the fluorophore flexibility to sample different microenvironments while bound to the agonist sites. Because it is known that the fluorescence lifetime of 1-(dimethylamino)-5-naphthalenesulfonamide is highly dependent on solvent polarity (Li et al., 1975), microenvironments that differ in polarity may give rise to different lifetimes.

Second, the uncorrected transfer efficiency calculated from lifetime data assuming Model I is identical to the transfer efficiency calculated by steady-state methods. In contrast, the transfer efficiencies calculated assuming Model II are not in agreement with the steady-state value. Therefore, since transfer efficiency values derived from steady-state measurements do not depend upon

assignment of Dansyl-C_6-choline lifetimes to the α_1 and α_2 subunits, the agreement between the values supports Model I.

Finally, we can consider the extreme case where all energy transfer would occur from one donor bound to one of two α-subunits, and the second donor would not participate in energy transfer. In this particular case, no change in the lifetime of the second donor and twice the change in the participating donor would be predicted (Cantley and Hammes, 1976). We can eliminate this extreme case from further consideration since irrespective of either Model I or II being correct, the reduction in both fluorescent lifetimes is indicative of nearly equal quenching occurring for bound DANSYL-C_6-choline at both (α_1 and α_2) α-subunit sites (Table VII). Thus, in either Model, a nearly symmetrical placement of the agonist sites with respect to the NCI site is indicated (Table IX).

The results of this study complement and extend previous efforts to localize the agonist and NCI sites. Snake neurotoxins have been widely used to localize the agonist sites. However, the α-toxins are quite large with dimensions of 20 x 30 x 40Å (Walkinshaw et al., 1980). Electron microscopy has shown that a portion of the toxin molecule is situated at the apex of the α-subunit (Kistler et al., 1982). Localization of the central loop has been a focus of many studies since it is believed to overlie the agonist site (Juillerat et al., 1982). Using electron spin resonance spectroscopy, it was shown that the tip of the central toxic loop is in tight contact with the receptor (Bystrov et al., 1983).

The location of the toxin central loop was further resolved by measuring energy transfer between two fluorescent labelled α-toxins. A distance (R(2/3)) of about 67Å (R_{MIN} to R_{MAX} = 55-85Å) was calculated indicating that a portion of the toxin resides near the outer perimeter of the 70Å diameter receptor (Johnson et al., 1984). These results were confirmed and extended by measurements of

energy transfer between a fluorescent lysine 23-labeled toxin and decidium, a small fluorescent ligand which acts as an antagonist (Johnson et al., 1987). The latter study showed that these fluorophores are separated by at least 50Å and also suggested the lysine 23 binding area of the toxin and the fluorophore for decidium were located away from the central axis of symmetry on the receptor. The transverse position of the α-toxin lysine 23 region with respect to the membrane has been defined by energy transfer measurements between several fluorescent toxin derivatives and eosin alkylamide incorporated into the membrane. Analysis of this data indicates that this residue is at least 40Å above the plane of the membrane (Section II). Lysine 23 is located in the central toxic loop midway along the long 40Å axis of the toxin (Walkinshaw et al., 1980). The synaptic apex of the AcChR extends as much as 60Å from the extracellular surface of the bilayer. Consideration of the above distances suggests that the tip of toxic loop and therefore the agonist sites cannot be closer than 20Å to the bilayer surface (see Fig. 27).

Our data showing a near symmetrical placement of the NCI site with respect to the agonist sites is consistent with a large body of evidence indicating that NCIs bind within or near the central ion channel. First, a number of electrophysiological studies based upon voltage, noise, and single channel (Neher and Steinbach, 1978) analyses (Katz and Miledi, 1975) suggest that these compounds bind to a specific site within the open ion channel, physically occlude the pore and thereby block ion flux (Neher and Steinbach, 1978; Adams, 1977; Koblin and Lester, 1979). Several NCI ligands, including QX-222 (Neher and Steinbach, 1978), quinacrine (Tsai et al., 1979), and PCP (Papke and Oswald, 1986; Changeux et al., 1986) reduce the duration of channel open times. Recently, it has been shown that ethidium also blocks agonist-regulated currents

with some properties characteristic of an open channel blocker (R.J. Leonard, personal communication). Secondly, the kinetics of [^{3}H]PCP binding to the open channel state of the AcChR suggest a binding site within the ion channel (Oswald et al., 1983). Association rates for the open channel state are 10^3 - 10^4 fold greater than with the closed, desensitized state. In addition, the kinetics of covalent NCI ligand labeling of the open channel state occur with greatly enhanced rates (Heidmann and Changeux, 1984, 1986; Muhn et al., 1984; Cox et al., 1985).

Photoaffinity labeling experiments have shown that NCIs simultaneously label one or more subunits. For example, chlorpromazine labeled all four polypeptide chains with identical kinetics (Heidmann and Changeux, 1986). Thus, these biochemical studies indicate that the NCI site must be formed by a close apposition of all four types of subunits. Since electron microscopy has shown that the ion channel opening is wide throughout the synaptic surface (25-30Å diameter), it is likely that the NCI labeled site is in a narrow portion that traverses the membrane (Toyoshima and Unwin, 1988).

The above discussion highlights our knowledge of the structure of the AcChR and the uncertainties associated with defining the location of the agonist and NCI binding sites. Despite the uncertainties, a useful picture emerges from consideration of this body of data. First, we can place constraints on the locations of the agonist sites with regard to the central axis of the ion channel. The distance between the two agonist sites limits the transverse displacement of the NCI sites from the plane of the agonist sites. Fig. 26 depicts the transverse distances from the agonist sites to the NCI site as a function of the distance between the agonist sites. The range of possible values are plotted for the Dansyl-C_6-choline-ethidium (R(min), R(2/3) and R(max)

distances using the geometrical relationships of the Pythagorean theorem. The receptor structure defines a minimum possible distance between the agonist sites of 30Å which is the internal diameter of the wide-mouthed extracellular portion of the receptor (Fig. 26). Thus, the if the agonist sites are located on the inner walls of the α-subunits and we utilize the determined intersite distance (Model I R(2/3) value for Dansyl-C_6-choline/ethidium, then the NCI site would reside 28Å below the plane defined by the agonist sites.

The maximum possible distance between two agonist sites based solely upon receptor structural limitations is about 60Å. In order to satisfy symmetry conditions and have an agonist-NCI intersite distance of 32Å, this assumes all three sites to be nearly coplanar (Fig. 26). However, this spatial arrangement appears highly unlikely since it places the NCI site within the aqueous space defined by the 30Å diameter synaptic portion of the channel (Fig. 27). Furthermore, it is consistent with data that indicates that the NCI site reside near or within the transmembrane domain of the AcChR. Thus, as seen in Fig. 26, a distance between the agonist sites of 30Å to 50Å indicates the transverse distance from the agonist sites to the NCI site will be in the range of 20-30Å.

Several studies (Kistler et al., 1982; Klymkowsky and Stroud, 1979) have inferred from electron microscopy of gold-labeled antitoxin antibody-toxin-AcChR complexes or X-ray diffraction that the agonist binding sites are located on the synaptic apex of the AcChR, 55Å from the entrance to the ion channel. However, our data are inconsistent with this proposed location for the agonist binding sites and indicates a location closer to the membrane bilayer surface. Furthermore, the agonist site has been localized within the primary sequence by affinity labeling studies. Cys-192 and Cys-193 comprise part of the agonist binding site (Kao et al., 1984). According to models of AcChR structure, these

data would place the agonist site not too far (<30Å) from the beginning of the proposed M1 membrane spanning hydrophobic region (Ile-212) of the α-subunit.

Our model for the locations of the NCI and agonist sites within the overall AcChR structure is diagrammed in Fig. 27. In this model, the NCI binding site resides within the central transmembrane domain of the ion channel, close to the extracellular surface of the bilayer. Sequence analysis has shown that [^{3}H]-chlorpromazine is attached to serine 262 on the δ subunit (Oberthur et al., 1986). According to current models of AcChR structure, these residues are placed within the homologous hydrophobic segments termed M2 which are part of each subunit and are postulated to span the bilayer (Noda et al., 1983; Claudio et al., 1983; Devillers-Thiery et al., 1983; Finer-Moore and Stroud, 1984). In addition, it is interesting to note that there are a number of non-polar and hydrophobic residues within the M2 region that may contribute to the NCI site. These residues are highly conserved in the α, β, γ and δ subunits. Our analysis of the microenvironment of the NCI binding site in the desensitized AcChR state is consistent with this interpretation. We found that bound ethidium exhibited a long fluorescence lifetime, large spectral shifts, and a near maximal limiting polarization value which indicated that part of the binding site is a hydrophobic pocket and highly restrictive of molecular motion (Herz et al., 1987). Thus, our model is in general agreement with several models of AcChR structure that predict an uncharged hydrophobic α-helix contributing to walls of the ion channel.

Our study has yielded complementary information that further localizes the positions of critical functional residues within the important ligand binding sites on the AcChR. The advantage of this fluorescence approach is that it provides a means of mapping structure of the functional, intact protein. The use of small fluorescent ligands has allowed this analysis to provide a more accurate

localization of the binding sites than previous studies which have used larger molecules such as α-toxins or antibodies. While these studies do not conclusively establish that the site of ethidium binding is in the central ion channel, future energy transfer studies between the NCI site and the lipid membrane will enable us to localize its position with respect to the membrane layer.

BIBLIOGRAPHY

Adams, P.R. (1977) J. Physiol. (Lond.) 268, 291-318.

Agard, D.A. & Stroud, R.M. (1982) Acta Crystallogr. A38, 186-194.

Berman, H.A., Yguerabide, J., & Taylor, P. (1980) Biochemistry 19, 2226-2235.

Bienvenue, A., Rousselet, A., Kato,G., & Devaux, P.F. (1977) Biochemistry, 16, 841-848.

Bjellqvist, B. Ek, K., Righetti, P.G., Gianazza, E., Görg, A., Westermeier, R., & Postel, W. (1982) J. Biophys. Methods, 6, 317-339.

Bolger, M.B., Dionne, V., Chrivia, J., Johnson, D.A., & Taylor, P. (1984) Mol. Pharmacol. 26, 57-69.

Brisson, A. & Unwin, P.N.T. (1985) Nature 315, 474-477.

Bystrov, V.F., Tsetlin, V.I., Karlsson, E., Pashkov, V.S., Utkin, Y.N., Kondokov, V.I., Pluzhnikov, K.A., Arseniev, A.S., Ivanov,, V.T., & Ovchinnikov, Y.A. (1983) In Toxins as Tools in Neurochemistry (F. Hucho & Y.A. Ovchinnikov eds.), pp.171-191, Walter de Gruyter & Co., New York.

Cantley, L.C., & Hammes, G.G. (1976) Biochemistry 15, 1-8.

Changeux, J.P., Pinset, C., & Ribera, A.B. (1986) J. Physiol. (Lond.) 378, 495-513.

Changeux, J.-P., Devillers-Thiery, A., Chemouilli, P. (1984) Science 225, 1335-1345.

Changeux, J.-P., Girandt, J., & Dennis, M. (1987) Trends Pharmacol. Sci., 8 459-465.

Changeux, J.-P., Devillers-Thiery, A., & Chemouilli, P. (1984) Science, 224, 1335-1345.

Chen, R.F. (1965) Science, 150, 1593-1595.

Cheung, A.T., Johnson, D.A., & Taylor, P. (1984) Biophys. J., 45, 447-454.

Claudi, T., Bavillet, M., Patrick, J., & Heinemann, S. (1983) Proc. Natl. Acad. Sci. USA 80, 2067-2071.

Claudio, T., M. Ballivet, J. Patrick & S. Heinemann. (1983) Nature (Lond.), 80 1111-1115.

Cox, R.N., Kaldany, R.R.J., Di Paola, M., & Karlin, A. (1985) J. Biol. Chem. 260, 7186-7193.

Dale, R.E., Eisinger, J., & Blumberg, W.E. (1979) Biophys. J. 26, 161-194.

Damle, V.N. & Karlin, A., (1978) Biochemistry, 17, 2039-2045.

Devillers-Thiery, A., Giraudat, J. Bentaboulet, M., & Changeux, J.-P. (1983) Proc. Natl. Acad. Sci. USA 80, 2067-2071.

Dufton, M.J. & Hider, R.C. (1983) CRC Critical Reviews in Biochemistry 14, 113-171.

Fairclough, R.H., & Cantor, C.R. (1978) Methods Enzymol. 48, 347-379.

Finer-Moore, J., & Stroud, R.M. (1984) Proc. Natl. Acad. Sci. USA 81, 155-159.

Forster, T. (1965) in Modern Quantum Chemistry (Sinanoglu, O., ed.) Part 3, pp. 93-137, Academic Press, NY.

Forster, T. (1959) Discuss. Faraday Soc. 27, 7-17.

Giersig, M., Kunath, W., Sack-Kongehl, & Hucho, F. (1986) in Nicotinic Acetylcholine Receptor Structure & Function; Maelicke, A., ed., Springer-Verlag, Berlin.

Giraudat, J., Dennis, M., Heidemann, T., Chang, J.-Y., & Changeux, J.-P. (1986) Proc. Natl. Acad. Sci. USA 83, 2719-2723.

Giraudat, J., Dennis, M., Heidmann, T., Hammont, P.T., Lederer, F., & Changeux, J.-P. (1987) Biochemistry 26, 2410-2418.

Heidmann, T., & Changeux, J.-P. (1979) Eur. J. Biochem. 94, 255-279.

Heidmann, T., & Changeux, J.-P. (1984) Biochemistry 25, 6109-6113.

Heidmann, T., & Changeux, J.-P. (1984) Proc. Natl. Acad. Sci. USA 81, 1897-1901.

Heidmann, T., Oswald, R.E., & Changeux, J.-P. (1983) Biochemistry 22, 3112-3127.

Herz, J., Johnson, D.A., & Taylor, P. (1987) J. Biol. Chem. 262, 7238-7247.

Holowka, D. & Baird, B. (1983b) Biochemistry, 22 3474-3484.

Holowka, D. & Baird, B. (1983a) Biochemistry, 22 3466-3474.

Hucho, F., Oberthur, W., & Lottspeich, F. (1986) FEBS Lett. 205, 137-142.

Hucho, F. (1979) FEBS Lett. 103, 27-32.

Johnson, D.A., Voet, J.G., & Taylor, P. (1984) J. Biol. Chem. 259, 5717-5725.

Johnson, D.A., Brown, R.D., Herz, J.M., Berman, H.A., Andreasen, G.L., & Taylor, P. (1987) J. Biol. Chem. 262, 14022-14029.

Johnson, D.A. & Taylor, P. (1982) J. Biol. Chem. 257, 5632-5636.

Johnson, D.A. & Nguyen, L.Q. (1987) (unpublished).

Johnson, D.A. & Yugerabide, J. (1985) Biophys. J. 48, 949-955.

Johnson, D.A., Voet, J. G., & Taylor, P. (1984) J. Biol. Chem. 259, 5717-5725.

Johnson, D.A. & Cushman, R. (1988) J. Biol. Chem. 263, 2802-2807.

Juillerat, M.A., Schwendimann, B., Hauert, J., Fulpius, B.W., & Bargetzi, J.P. (1982) J. Biol Chem. 257, 2901-2907.

Kaldany, R., & Karlin, A. (1983).

Kao, P.N., Dwork, A.J., Kaldany, R.J., Silver, M.L., Wideman, J., Stein, S., & Karlin, A. (1984) J. Biol. Chem. 259, 1162-1165.

Karlin, A. (1980) in The Cell Surface & Neuronal Function (G. Poste, G. Nicolson, & C. W. Cotman, eds.) Raven Press, New York, 141-260.

Karlson, E., D. Eaker, & G. Ponterius (1972) Biochim. Biophys. Acta 257

235-248.

Karlsson, E., Arnberg, H., & Eaken, D. (1971) Eur. J. Biochem. 21, 1-16.

Kistler, J., Stroud, R.M., Klymkowsky,, M.W., Lalancette, R.A., & Fairclough, R. H. (1982) J. Biophys. 37, 371-383.

Kubalek, E., Ralston, S., Lindstrom, J., & Unwin, N. (1987) J. Cell Biol.105, 9-18.

Lehrer, S., Graceffa, P., & Betteridge, D. (1981) Ann. N.Y. Acad. Sci. 366, 285-296.

Lentz, T.L., Hawrot, E., & Wilson, P.T. (1987) Proteins: Struc., Func., Genet. 2, 298-307.

Li, Y.-H., Chan, L.-M., Tyer, L., Moody, R.T., Himel, C.M., & Hercules, D.M. (1975) J. Am. Chem. Soc. 97, 3118-3126.

Lobel, P., Kao, P., Birken, S., & Karlin, A. (1985) J. Biol. Chem. 260, 10605-10612.

Low, B.W. (1979) Handb. Exp. Pharmacol. 52, 213-257.

Low, B.W., Preston, H.S, Sato, A., Rorsen, L.S., Searl, J.E., Ruddko,, A.D., & Richardson, J. S.(1976) Proc. Natl. Acad. Sci. U.S.A. 73, 2991-2994.

Lowry, O.H., Rosenbrough, N.J., Farr, A. L., & Randoll, R.J, (1951) J. Biol. Chem. 193, 265- .

Matsumoto, S., & Hammes, G.G. (1975) Biochemistry 14, 214-224.

Muhn, P., & Hucho, F. (1983) Biochemistry 22, 421-425.

Muhn, P., Fahr, A., & Hucho, F. (1984) Biochemistry 23, 2725-2730.

Nathanson, N.M. & Hall, Z.W. (1980) J. Biol. Chem. 255, 1698-1703.

Neher, E., & Steinbach, J.H. (1978) J. Physiol. (Lond.) 277, 153-176.

Neubig, R.R., Krodel, E.K., Boyd, N.D., & Cohen, J.B. (1979) Proc. Natl. Acad. Sci., 76, 690-694.

Noda, M., Takahashi, H., Tanabe, T., Toyosato, M., Kikyotani, S., Hirose, T. Asai, M., Takashima, H., Inayam, S., Miyata, T., & Numa, S. (1983) Nature (Lond.) 301, 251-255.

Noda, M., Takahashi, H., Tanabe, T., Toyosato, M., Furutani, Y., Hirose, T., Asai, M., Inayama, S., Miyata, T., & Numa, S. (1982) Nature 299, 793-797.

Noda, M., Takahashi, H., Tanabe, T., Toyosato, M., Kikyotani, S., Furutani, Y., Hirose, T., Takashima, H., Inayam, S., Miyata, T., & Numa, S. (1983) Nature 302, 528-532.

Oberthur, W., Muhn, P., Baumann, H., Lottspeich, F., Wittmann-Liebold, B., & Hucho, F. (1986) EMBO J. 5, 1815-1819.

Oswald, R.E. & Changeux, J.-P. (1982) FEBS Lett. 139, 225-229.

Oswald, R., & Changeux, J.-P. (1981) Proc. Natl. Acad. Sci. USA 78, 3925-3929.

Oswald, R., Heidmann, T., & Changeux, J.-P. (1983) Biochemistry 22, 3128-3136.

Parker, C.A. & Rees, W.T. (1960) Analyst, 85, 587- .

Ralston, S., Sarin, V., Thanh, H.L., River, J., Fox, J.L., & Lindstrom, J. (1987) Biochemistry, 26, 3261-3266.

Reed, K., Vandlen, P., Bode, J., Duguid, J., & Raftery, M.A. (1975) Arch. Biochem. Biophys. 167, 138-144.

Schiller, P.W. (1975) in Biochemical Fluorescence (Chen, R.F. & Edelhoch, H. Eds.) Vol. 1, pp 285-303, Marcel Dekker, New York.

Schmidt, J. & Raftery, M.A. (1973) Anal. Biochem. 52, 349-355.

Shaklai, N., Yguerabide, J., & Ranney, H.M. (1977) Biochemistry 16, 5585-5592.

Tan, Y. & Barrantes, F.J. (1980) Biochem. Biophys. Res. Comm., 92, 766-774.

Toyoshima, C., & Unwin, N. (1988) Nature 336, 247-250.

Tsernoglou, D., Petsko, G.A., & Hudson, R.A.(1978) Mol. Pharmacol. 14, 710-716.

Unwin, N., Toyoshima, C., & Kubalek, E. (1988) J. Cell Biol. 107, 1123-1138.

Waksman G., Changeux, J.P., & Rogues, B.P. (1980) Mol. Pharm. 18, 20-27.

Walkinshaw, M., Saenger, W., & Maelicke, A. (1980) Proc. Natl. Acad. Sci. USA 77, 2400-2404.

Weiland, G., Georgia,, B., Lappi, S., Chignell, C. F., & Taylor, P. (1977) J. Biol. Chem., 252, 7648-7656.

Wilson, P.T. & Lentz, T.L. (1988) Biochemistry, 27, 6667-6674.

Witzemann, V., Muchmore, D., & Raftery, M.A. (1979) Biochemistry 18, 5512-5518.

Wolber, P.K. & Hudson, B.S. (1979) Biophys J. 28, 197-210.

Yguerabide, J. (1972) Methods Enzymol. 26, 498-578.

Yguerabide, J., & Yguerabide, E.E. (1984) in Optical Techniques in Biological Research (Doyle, J., ed.) pp. 181-290, Academic Press, Orlando, FL.

Zingsheim, H.P., Barrantes, F.J., Frank, J., Hänicke, W., & Neugebauer, D.-Ch. (1982) Nature 299, 81-84.

LIST OF ABBREVIATIONS

α-toxin	Naja naja siamensis 3 α-toxin
σ	surface density as number of acceptors/Å^2.
AcChR	nicotinic acetylcholine receptor
E_A	energy transfer efficiency
FITC	fluorescein isothiocyanate
FITC-lys-23-toxin	$N_\epsilon$fluorescein-lysine-23-α-toxin
FITC-lys-35-toxin	$N_\epsilon$fluores cein-lysine-35-α-toxin
FITC-lys-49-toxin	$N_e$fluorescein-lysine-49-α-toxin
FITC-lys-69-toxin	$N_\epsilon$fluorescein-lysine-69-α-toxin
FITC-toxin	mono-FITC α-toxin derivative
HPLC	high pressure liquid chromatography.
I_b	fluorescence intensity of the AcChR-bound fluorophore
I_e	equilibrium fluorescence intensity
I_f	fluorescence intensity of fluorophore free in solution
IPG	immobilized pH gradients
J	overlap integral
κ^2	orientation factor
k_{FQ}	bimolecular quenching rate constant
K_Q	Stern-Volmer quenching constant;
L	distance of closest approach between lipid-membrane surface and AcChR-bound fluorophore
PCP	phencyclidine
Q	quantum yield
Q_D	donor quantum yield
Q_{DA}	donor quantum yield in presence of acceptor
R_o	Forster critical distance
TFA	trifluoroacetic acid
TRITC	tetramethylrhodamine isothiocyanate